LA-UR-15-26804
Approved for public release; distribution is unlimited.

Title: Brine Transport Experiments in Granular Salt

Author(s): Jordan, Amy B.
Boukhalfa, Hakim
Caporuscio, Florie Andre
Stauffer, Philip H.

Intended for: DOE-NE deliverable
Report

Issued: 2016-06-06 (rev.1)

Brine Transport Experiments in Granular Salt

Fuel Cycle Research & Development

Prepared for
U.S. Department of Energy
Used Fuel Disposition Campaign
Milestone M4FT-15LA0819013

A.B. Jordan, H. Boukhalfa , F.A. Caporuscio, P.H. Stauffer,
Los Alamos National Laboratory
August 31, 2015

Los Alamos National Laboratory Document
LA-UR-15-26804

FCT Quality Assurance Program Document

Appendix E
FCT Document Cover Sheet

Name/Title of Deliverable/Milestone	LANL Report entitled - "Brine Transport Experiments in Granular Salt "
Work Package Title and Number	DR Salt Field Testing – LANL, FT-15LA081901
Work Package WBS Number	**1.02.08.19**
Responsible Work Package Manager	Philip Stauffer (Name/Signature)
Date Submitted	August 2015

Quality Rigor Level for Deliverable/Milestone	☒ QRL-3	☐ QRL-2	☐ QRL-1 ☐ Nuclear Data	☐ N/A*

This deliverable was prepared in accordance with Los Alamos National Laboratory

(Participant/National Laboratory Name)

QA program which meets the requirements of

☒ DOE Order 414.1 ☐ NQA-1-2000

This Deliverable was subjected to:

☐ Technical Review

Technical Review (TR)

Review Documentation Provided

☐ Signed TR Report or,

☐ Signed TR Concurrence Sheet or,

☐ Signature of TR Reviewer(s) below

Name and Signature of Reviewers

HARI VISWANATHAN

☒ Peer Review

Peer Review (PR)

Review Documentation Provided

☐ Signed PR Report or,

☐ Signed PR Concurrence Sheet or,

☒ Signature of PR Reviewer(s) below

*Note: In some cases there may be a milestone where an item is being fabricated, maintenance is being performed on a facility, or a document is being issued through a formal document control process where it specifically calls out a formal review of the document. In these cases, documentation (e.g., inspection report, maintenance request, work planning package documentation or the documented review of the issued document through the document control process) of the completion of the activity along with the Document Cover Sheet is sufficient to demonstrate achieving the milestone. QRL for such milestones may be also be marked N/A in the work package provided the work package clearly specifies the requirement to use the Document Cover Sheet and provide supporting documentation.

EXECUTIVE SUMMARY

To gain confidence in the predictive capability of numerical models, experimental validation must be performed to ensure that parameters and processes are correctly simulated. The laboratory investigations presented herein aim to address knowledge gaps for heat-generating nuclear waste (HGNW) disposal in bedded salt that remain after examination of prior field and laboratory test data. Primarily, we are interested in better constraining the thermal, hydrological, and physicochemical behavior of brine, water vapor, and salt when moist salt is heated (*Jordan et al.*, 2014; *Stauffer et al.*, 2015). The target of this work is to use run-of-mine (RoM) salt; however during FY2015 progress was made using high purity, granular sodium chloride.

Coupled thermal/hydrological/chemical (THC) modeling performed to date has demonstrated that under certain conditions, enhanced heat transfer through water vapor transport may be sustained in crushed salt backfill around a heat source at temperatures relevant to high-level waste. Perturbations in thermal transport through vapor/liquid cycling may lead to significant porosity and permeability change, and a substantial impact on the predicted temperature and moisture state of the system. Model verification and validation are required to better understand the role of vapor transport in HGNW.

The experiments described in this report take place under representative generic salt repository conditions at the laboratory scale using uniform grain size granular salt. There are two primary objectives to the experimental effort: (1) understanding and quantifying specific physical processes that may operate during disposal of heat-generating nuclear waste (HGNW) in drifts or alcoves backfilled with rubblized salt; and (2) validating numerical models that attempt to represent associated flow and transport processes.

Three experiments were performed. The first was a preliminary run-through for testing of equipment and procedures, but it also provided useful results about water vapor migration under conditions of varying airflow. In particular, the relative humidity rebound curve showed hysteretic effects as time progressed, indicating that the hygroscopic behavior of the salt in the box leads to differences in water vapor migration as the system approaches equilibrium. A tracer test with chloroform was performed for comparison with the water vapor/relative humidity rebound curve. The next two experiments involved heating of the salt using a variable thermal output block heater in the presence of a small ponded water layer at the bottom of the experimental box. These tests included multiple tracer runs with chloroform and SF_6. The breakthrough curves show that tracers may be used to interrogate internal structural changes in the salt during an experiment and indicate the timing of porosity change. Over the course of 3 weeks, breakthrough curves for chloroform and SF_6 became significantly more delayed, requiring smaller effective tortuosities to fit the data with a simple analytical solution to the advection-dispersion equation, suggesting an increase in salt reconsolidation which was verified through post-test forensics. Results from the final experiment show thermal effects indicative of vapor/liquid cycling, where higher temperatures were seen on the face of the experimental box for a lower heat load, and internal temperatures within the experimental box showed a region with a very shallow thermal gradient.

Lessons learned during this first phase of experimentation and the observed results suggest a path forward for additional experiments. After the desired experimental test runs with granular salt, the procedures developed and lessons learned while using the granular salt will be applied to a similar experiment using screened RoM salt from the Waste Isolation Pilot Plant.

TABLE OF CONTENTS

1. INTRODUCTION 1

1.1 OBJECTIVES 1

1.2 BACKGROUND 2

2. METHODS 6

3. RESULTS AND DISCUSSION 12

3.1 TEMPERATURE DISTRIBUTION 12

3.2 TRACER TESTS 15

3.3 POST-TEST FORENSICS 27

3.4 WATER VAPOR BEHAVIOR 32

4. CONCLUSIONS 34

5. FUTURE WORK 35

REFERENCES 37

LIST OF FIGURES

FIGURE 1: HEAT PIPE IN SALT. 4
FIGURE 2: (A) SALT BOX, DATA LOGGERS, AND MULTI-GAS MONITOR. (B) SETUP SHOWING THE APPARATUS FOR AIRFLOW OF KNOWN RELATIVE HUMIDITY (FROM THE HOUSE AIR) THROUGH THE BEAKER ON THE COUNTER, MONITORED WITH A RELATIVE HUMIDITY SENSOR, THROUGH THE LID OF THE BOX. 6
FIGURE 3. LOCATION OF THERMOCOUPLE BUNDLES. BUNDLE A IS 1 IN. FROM THE HEATER'S LONG EDGE; B IS 3.25 IN.; AND C IS 6.75 IN. 7
FIGURE 4. SCHEMATIC OF THE EXPERIMENTAL SETUP. SOME MEASUREMENTS ARE NOT INDICATED HERE BECAUSE THE PLACEMENT OF COMPONENTS VARIED BETWEEN EXPERIMENTS. 8
FIGURE 5. EXPERIMENT 1 SETUP SHOWING HEATER CONTROLLER, INJECTION PORT, AND PONDED WATER LINE. A SLIGHT RISE IN THE INJECTION PORT STAINLESS STEEL TUBE KEEPS IT ABOVE THE PONDED WATER LINE. 10
FIGURE 6. TEMPERATURE WITH TIME FOR THE THERMOCOUPLES OF BUNDLE A (CLOSEST TO HEATER). THERMOCOUPLE A7 IS THE SHALLOWEST IN THE SALT AND A1 IS THE DEEPEST. HEATER TEMPERATURE IS 260^{O}C. 12
FIGURE 7. STEADY-STATE TEMPERATURE DISTRIBUTION WITH DEPTH FOR EXPERIMENTS 1 AND 2. THE DISTANCE FROM THE THERMOCOUPLE BUNDLE TO THE HEATER IS INDICATED. 13
FIGURE 8. INFRARED IMAGES TAKEN 5/4/15 (EXPERIMENT 1) OF (A) THE SALT BOX FACE PARALLEL TO THE LONG EDGE (5") OF THE HEATER AND (B) PARALLEL TO THE SHORT EDGE (2") OF THE HEATER. PHOTOS COURTESY OF HANK HERBER. 14
FIGURE 9. INFRARED IMAGES TAKEN 7/21/15 (EXPERIMENT 2) OF THE SALT BOX FACE PARALLEL TO THE LONG EDGE OF THE HEATER, AS IN FIGURE 8(A). PHOTO COURTESY OF HANK HERBER. 14
FIGURE 10. CONCEPTUAL DIAGRAM OF THE TRACER TRANSPORT MODEL. DOWNWARD FLOW (DASHED ARROWS) IS NOT MODELED. 15
FIGURE 11. ANALYTICAL SOLUTION (EQUATION 3) FOR GAS PHASE CONCENTRATION OF SF_6 IN THE SALT AT Z = 42 CM, T = 5 HOURS, NORMALIZED BY PEAK CONCENTRATION. 16
FIGURE 12. SCHEMATIC OF THE AIR MIXING MODEL. 17
FIGURE 13. (A) CHLOROFORM DIMENSIONLESS HENRY'S LAW COEFFICIENT, $H_D = C_L/C_G$, AS A FUNCTION OF TEMPERATURE (SANDER, 2015). (B) FREE-AIR DIFFUSION COEFFICIENT OF SF_6 (WATTS, 1971) AND CHLOROFORM (MARRERO AND MASON, 1972) AS A FUNCTION OF TEMPERATURE. 18
FIGURE 14. SCHEMATIC OF TRACER TESTS PERFORMED DURING EXPERIMENT 1. NOTE THAT THE INTERIOR STRUCTURE DEPICTED IN THE POST-TEST SCENARIO IS FOR ILLUSTRATION ONLY AND IS NOT INTENDED TO BE REPRESENTATIVE OF THE OBSERVED POROSITY DISTRIBUTION. 19
FIGURE 15. CHLOROFORM BREAKTHROUGH CURVES, BOTH DATA AND MODELED, FOR THE PRE-TEST COOL TRACER RUN (T1-COOL ON 4/22/15), AND THE FIRST AND SECOND HEATED TRACER TESTS (T2-HOT ON 4/27/15 AND T3-HOT ON 4/30/15) 20
FIGURE 16. CHLOROFORM BREAKTHROUGH CURVES, BOTH DATA AND MODELED, FOR THE PRE-TEST COOL TRACER RUN (T1-COOL ON 4/22/15) AND FINAL POST-TEST COOL RUN (T5-COOL ON 5/11/15). 22
FIGURE 17. CHLOROFORM BREAKTHROUGH CURVES, BOTH DATA AND MODELED, FOR THE HEATED CASES (T2-HOT ON 4/27/15; T3-HOT ON 4/30/15; AND T4-HOT ON 5/07/15). THE COOL CASES OF FIGURE 16 (T1, PRE-TEST AND T2, POST-TEST) ARE SHOWN IN GRAY FOR COMPARISON. 23
FIGURE 18. CHLOROFORM AND SF_6 BREAKTHROUGH CURVES, BOTH DATA AND MODELED, FOR T4-HOT ON 5/07/15 AND T5-COOL ON 5/11/15. 24
FIGURE 19. CHLOROFORM AND SF_6 BREAKTHROUGH CURVES, BOTH DATA AND MODELED, FOR T2-1-COOL ON 7/16/15 AND T2-2-HOT ON 7/17/15 25
FIGURE 20. EXCAVATION OF EXPERIMENT 0; OBSERVATIONS OF ZONES OF SALT CONSOLIDATION 28
FIGURE 21. MOISTURE CONTENT WITH DEPTH IN THE EXCAVATED EXPERIMENT 0 SALT BOX. 28
FIGURE 22. DISCOLORED REGION AROUND THE HEATER. SOME VERY SLIGHT CONSOLIDATION WAS OBSERVED, AS WELL AS SOME LOOSENESS OF THE SALT IMMEDIATELY SURROUNDING THE HEATER. THE LOOSE REGION WAS SIGNIFICANTLY FIRMER AND SMALLER THAN IN EXPERIMENT 0 (FIGURE 20). 29
FIGURE 23. TOUGH RIND ALONG THE EDGES OF THE SALT BOX. 29
FIGURE 24. MOISTURE CONTENT WITH DEPTH IN THE EXCAVATED EXPERIMENT 1 SALT BOX. 30

FIGURE 25. TRANSMITTED LIGHT IMAGE OF SAMPLE SS-22 SHOWING DISSOLUTION AND RE-PRECIPITATION OF SALT GRAINS IN SAMPLE. 31
FIGURE 26. RELATIVE HUMIDITY IN THE AIRSPACE DURING EQUIPMENT AND VENTILATION TESTING (EXPERIMENT 0). IN BOTH CASES THE AIRFLOW IS STOPPED ON DAY 0. PONDED WATER AT THE BOTTOM OF THE SALT BOX PROVIDES A MOISTURE SUPPLY AND THE AIRSPACE RELATIVE HUMIDITY CLIMBS IN THE ABSENCE OF VENTILATION. 33
FIGURE 27. CHLOROFORM BREAKTHROUGH DURING EXPERIMENT 0 DURING A TEST WITH NO AIRFLOW. 34

LIST OF TABLES

TABLE 1: PROPERTIES OF SOLID SALT GRAINS AND BULK VALUES. 7
TABLE 2. DIMENSIONS AND LOCATIONS OF APPARATUS IN THE SALT LABORATORY EXPERIMENTS. 8
TABLE 3. EXPERIMENT OVERVIEW 9
TABLE 4. TIMELINE OF EVENTS FOR EXPERIMENT 1. 11
TABLE 5. TIMELINE OF EVENTS FOR EXPERIMENT 2. 11
TABLE 6: BREAKTHROUGH CURVE FITTING MODEL PARAMETERS. 19
TABLE 7. SUMMARY OF RESULTS FROM THE BEST FITS TO THE TRACER BREAKTHROUGH MODEL. 24
TABLE 8. CALCULATED POROSITY AND PETROGRAPHIC DESCRIPTION OF DISSOLUTION/ PRECIPITATION BEHAVIOR. 32

Brine Transport Experiments in Granular Salt

1. Introduction

Unanswered questions regarding subsurface transport of liquid water and water vapor are the motivation for current and future experimental efforts (*Jordan et al., 2014; Stauffer et al.,* 2015). Despite a strong basis of knowledge from prior studies (*Kuhlman and Malama,* 2013; *Kuhlman and Sevougian,* 2013), uncertainty can still be reduced for high-temperature heat-generating nuclear waste (HGNW) disposal in bedded salt in order to augment to existing safety case. Salt is an attractive material for a HGNW repository because of its properties. Although long-term isolation of waste is dominated by self-sealing viscoplastic salt reconsolidation and room closure (*Hansen and Leigh,* 2011), an understanding of short term behavior is necessary to make predictions about future field tests that will be required as part of any new underground storage facility.

Understanding and reducing uncertainties in the short-term behavior of brine, water vapor, and solid salt in the vicinity of the waste canisters is the focus of this report. Because HGNW will generate a much higher heat load than low-level waste, and because the behavior of salt (including reconsolidation) is highly dependent on temperature, improved representations of multiphase transport are necessary for the strongly coupled thermal, hydrological, mechanical, and chemical (THMC) processes acting in bedded salt. This research is site-independent and will fill science gaps that apply to any potential salt HGNW repository setting (*Robinson et al*., 2012).

1.1 Objectives

There are two primary objectives to the experimental effort developed as part of this research: (1) understanding specific physical processes that may operate during disposal of HGNW in drifts or alcoves with backfilled rubblized salt, and during full-scale heater experiments, that can be observed under controlled conditions in the laboratory; and (2) validating numerical models that attempt to represent associated flow and transport processes. Each is described in greater detail below.

For objective 1, a thorough understanding of the physical processes operating in a heated, moist salt environment is required to understand the safety of HGNW disposal in salt formations. While prior research has been done on many aspects of hydrogeological processes in porous media, less data exist for these same processes in salt with a saturated brine. To date, few dedicated laboratory experiments have been performed on granular salt material under relevant temperatures and moisture conditions. Processes to be studied in the bench-scale experiment include brine and water vapor movement in porous granular salt around a heater, including the extent of porosity change, the hygroscopic behavior of salt, water vapor loss into ventilated air space, and the thermal properties of granular salt. Open questions include whether vapor transport is advection or diffusion dominated for temperatures relevant to HGNW; how much water vapor retardation is expected due to deliquescence and how that changes with time as the system approaches equilibrium; how porosity and permeability are modified under heated as well as unheated conditions (due to salt deliquescence and reconsolidation); and whether gas-phase tracers can be used to interrogate internal structural changes during salt experiments at various scales.

The validation of physicohemical and hydrologic parameters and processes is the second objective of the experimental work. The observed spatial and temporal change of porosity, temperature, and moisture will be compared to numerical predictions. The comparisons will be used to assess all sub-models and assumptions used in the numerical simulations. Currently, data gaps exist in the following physical processes as represented: evaporation rate as a function of temperature, relative humidity, saturation in the run-of-mine (RoM) salt, and air turnover rate; water vapor diffusivity in porous RoM backfill; thermal models in RoM salt and air, with parameters such as emissivity for radiative heat transfer considered highly uncertain; relative permeability and capillary suction parameters; and the effect of compaction during porosity reduction.

It is not expected that the small-scale laboratory results will produce identical effects when upscaled to the repository level. Instead, these bench-scale experiments provide validation of the numerical models at the same scale, which will be used to design and predict results of larger intermediate- and field-scale heater experiments, which will then be validated with data at that scale (*Stauffer et al.*, 2015). In a feedback loop between the numerical model, laboratory experiments and field-scale experiments, experimental results will be used to validate the model, while the model will be used to interpret the field results. Together, the experiments and models will be the key to understanding the processes and evolution of a system for disposal of HGNW in bedded salt formations.

Knowledge gained from this research into the coupled processes in salt will be highly applicable to potential salt formation repositories worldwide. Most of our in-situ data for bedded salt come from the Waste Isolation Pilot Plant (WIPP) in Carlsbad, NM; however, our results are general and would be applicable to the siting of a salt repository in one of multiple suitable locations.

1.2 Background

Experimental, theoretical, and modeling investigations into nuclear waste storage in salt have been performed since before the 1960s (*Hansen and Leigh*, 2011). Heater tests have taken place in salt mines in Kansas, Louisiana, Germany, and at WIPP, but few past field experiments have reached temperatures as high as is possible for HGNW (200–300ºC). Several natural and man-made analogues to hot waste storage have also been studied, e.g., magmatic intrusion into salt formations and underground nuclear weapon tests in salt (*Hansen and Leigh*, 2011). At Yucca Mountain, the original proposed repository in tuff for the nation's HGNW, field-scale heater experiments were performed and an extensive modeling effort was undertaken (e.g., *Pollock et al*., 1986; *Rutqvist et al*., 2005; *Bodvarsson et al*., 1999).

Heat in HGNW is generated by fission products such as Cs-137, Sr-90, and alpha decay of actinides, with the primary contributors to the heat load changing over time (*Hansen and Leigh*, 2011). An ideal geologic repository setting would be in a medium with a high thermal conductivity, so that heat is transported away from the waste and extremely high temperatures do not build up around the source. Intact halite has a relatively high thermal conductivity (~5.5 W/m K) compared to other possible repository materials (*Hansen and Leigh*, 2011), but effective thermal conductivity is strongly dependent on temperature, porosity, and saturation. The crushed RoM salt material used as backfill over the waste canisters in the in-drift waste disposal concept, with its high porosity, initially has a much lower thermal conductivity (~0.7 W/m K) than intact salt (*Clayton and Gable*, 2009). However, the viscoplastic behavior of salt leads to porosity

reduction over time, and the properties of reconsolidated crushed salt are expected to eventually return to similar values as intact salt.

Sources of water in bedded salt and in RoM salt backfill include pore fluid (intergranular water) as well as bound water. Bound water sources within intact salt crystals (intragranular) are fluid inclusions of typical size 2–250 microns (*Kelly*, 1985), which impart minor saturations of ~0.1–1% (*Robinson et al*., 2012). More significant "bound" water includes clay layers and hydrate water in impurities commonly found in bedded salt formations (*Caporuscio et al.*, 2013). "Free" water sources include releases of water from those structurally bound sources (e.g., dehydration of the clay layers), as well as releases from the waste packages and from external sources; and condensation from the gas phase. In the subsurface, free fluids migrate under the influence of gravity, capillary forces, and stress, pressure, and temperature gradients. Fluid migration may contribute to mechanical weakening of the salt (*Urai et al*., 1986), as well as porosity and permeability changes (e.g., if brine in equilibrium with one temperature migrates to a warmer region and dissolves additional salt).

The bound fluids migrate as well, from factors such as pore collapse, grain boundary sliding associated with salt creep, dynamic recrystallization during dislocation creep, fracturing, decrepitation, and from temperature gradients. (Decrepitation is the violent fracturing of salt crystals which occurs around 280°C due to the pressure of heated brine; *Kelly*, 1985). The exact temperature of decrepitation depends on the particular material composition. In laboratory experiments, it is observed to cause a significant transfer of fluid from intra- to intergranular porosity (*Kuhlman and Malama*, 2013).

Water vapor transport plays a significant role in moisture redistribution in rubblized salt. While intact salt is nearly impermeable to gas flow, permeability and porosity in crushed salt will initially be quite high. Within pores, water partitions between the liquid phase and the vapor phase in an amount determined by temperature, pressure, and ion concentration in the liquid (*Stauffer et al*., 2013).

Between pores, movement of water vapor occurs by advection and diffusion, greatly modified by the presence of liquid saturation and the hygroscopic behavior of salt grains. The free-air diffusivity should be modified by a tortuosity term (τ) that may depend on porosity and saturation. Enhanced vapor diffusion is another saturation-dependent process that may affect water vapor transport in a repository setting. Normally, increasing saturation increases the tortuous path length for diffusion, decreasing the coefficient τ and the effective diffusivity. However, enhanced vapor diffusion in soils due to the presence of many little liquid islands was proposed even before direct evidence existed (*Ho and Webb*, 2006). Water condenses on the upgradient side of liquid islands and evaporates on the other side; the condensable particles in question (water or, e.g., isotopic tracers such as D_2O) migrate through the liquid islands at a faster rate than diffusion through a tortuous porous medium alone. The effect has been seen in a pore-scale experiment (*Silverman*, 1998). In a salt repository setting, thermal gradients and vapor pressure lowering may increase the potential for enhanced vapor diffusion.

Loss of water vapor from the salt pile occurs by evaporation and diffusion across the RoM/air boundary. Water loss from the salt pile will depend on the concentration gradient between water vapor in the "unventilated" pores (diffusion), advection from the salt pile into the air, and evaporation that depends on relative humidity, temperature, and water availability at the

surface of the pile (replenishment by suction). Ventilated air flow in the drift may allow efficient removal of water vapor.

Temperatures around the waste may exceed the boiling point of brine, and if conditions are conducive to it, a heat pipe may be established in the crushed salt backfill (Figure 1). In a heat pipe, water is vaporized in the boiling region, advects and diffuses along concentration gradients to the cooler regions where it recondenses, and replenishment of fluid towards the heat source is established from gravity flow and capillary pressure gradients (*Udell*, 1985; *Doughty and Pruess*, 1990). Water sources in the system that may feed the heat pipe include free pore fluids in the RoM salt, inflow from the DRZ into the RoM backfill, release of water from hydrous minerals, and, potentially, fluid inclusion migration up a temperature gradient. If a heat pipe is established, the result is a higher apparent or effective thermal conductivity and flatter temperature gradients around the waste (*Udell*, 1985; *Birkholzer*, 2004), lower maximum temperatures, and buildup of a low-porosity rind from evaporating brine in the boiling region (*Stauffer et al.*, 2013).

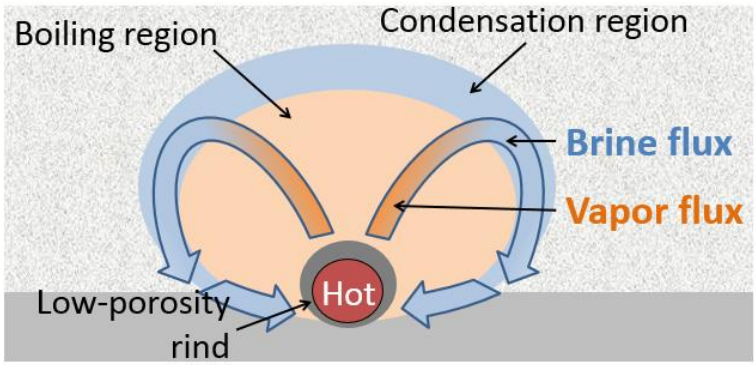

Figure 1: Heat pipe in salt.

It is not well-known whether heat pipe effects are likely to be present in a typical bedded salt repository for HGNW, due to spatial heterogeneities in water content, seepage rates, and impurity fractions. Dry-out of the crushed salt backfill could prevent potential heat pipe behavior, particularly during the operational ventilated period. Vapor flow may also be affected by barometric pumping or pressure differentials between the waste drift and the access drifts.

There is experimental evidence for porosity change from brine evaporation during 1980s heater tests at WIPP (*Krumhansl et al.*, 1991). After heating to up to 130^{o}C, heaters in both open boreholes and boreholes backfilled with crushed salt were found to be enclosed in solid rock salt with final bulk density within 99% of that of intact salt (2160 kg/m^{3}) (*Brady et al.*, 2013). The in-situ appearance of a rind from brine evaporation provides the primary motivation for studying the phenomenon in much greater detail to gain an understanding of whether such features are likely to form during HGNW repository operation.

Other field experimental studies of brine migration and salt behavior have been performed at WIPP, Avery Island, and Asse, Germany (*Kuhlman and Malama*, 2013). One focus of several prior in-situ experiments was the rate of brine migration to openings, which was found to be highly variable even within the same repository, due to geologic heterogeneity. A major effort to understand backfill material (i.e., crushed or rubblized salt) was undertaken in the domal salt

Asse repository. Known as the Backfill and Material Behavior in Underground Salt Repositories (BAMBUS) project, it included a drift-scale 9-year-long test (1990-1999) with heater canisters covered with crushed salt backfill, and associated laboratory testing and analysis. In-situ humidity monitoring was performed within the salt. The BAMBUS II follow-on project involved laboratory investigations and further forensic analysis of the prior in-drift experiment (*Bechthold et al*., 2004), because the first round of experiments had produced variable results. The BAMBUS results focused on salt reconsolidation, and found an approximately 10% porosity reduction after 10 years of heating.

While there have been laboratory experiments on compacted and intact salt from WIPP and other locations (*Kuhlman and Malama*, 2013), few laboratory experiments have been performed on crushed RoM-like material. The most relevant prior laboratory work on heated crushed salt is an experiment by *Olivella et al*. (2011), where a heat pipe was established in a 5 cm by 10 cm cylindrical apparatus with fixed temperature plates on both ends and a closed system for mass. Porosity change was observed along the length of the cylinder, with dissolution at the condensation front and buildup of a low-porosity rind. They provided destructive testing of the system at various times (7, 15, 30, and 65 days) to determine the spatial and temporal pattern of porosity change and saturation, and compared model results to the experimental. The experimental results were well-matched by the numerical model CODE-BRIGHT for the same scenario (*Olivella et al.*, 2011).

Other laboratory experimental investigations of heat pipes have been performed, but not in salt (e.g., *Udell*, 1985). The phenomenon was also observed at Yucca Mountain during a field heater test (*Birkholzer and Tsang*, 2000). The key difference between a heat pipe in salt versus other media is its three-phase nature. That is, besides liquid and vapor movement, precipitation and dissolution leads to solid redistribution as well. The added complexity of the strongly coupled thermal/hydrological processes associated with porosity change are a primary reason additional research is necessary into high-temperature, variably saturated salt.

Gas breakthrough testing in salt has been performed for compacted salt, but not for the more granular RoM in the early stages (first few years) following HGNW disposal. During the laboratory experiments described by *Cinar et al.* (2006), granular salt (pure NaCl) was deliberately compacted to low porosities (down to 4.7%) to accelerate the decades-long process of mechanical change that is expected in a salt repository. They performed porosity and permeability measurements on cm-scale core samples using gas flow measurements and a mercury porosimeter. They also obtained capillary pressure curves as a function of saturation for draining and imbibition. Laboratory gas permeability testing of samples from WIPP and Germany has also been performed (*Kuhlman and Malama*, 2013).

More common (both in the U.S. and other countries, e.g., Germany) than laboratory physiochemical and hydrologic testing in granular salt are mechanical and compaction studies, which are necessary for understanding the rates at which RoM salt will deform and what factors impede or enhance reconsolidation (e.g., *Urai et al.*, 1986). Prior experiments to test water loss and evaporation in natural systems (e.g., with lysimeters) are plentiful, but typically are focused on effects such as radiation and insolation, evapotranspiration and the effects of crop cover, etc. Even for bare-soil experiments, the difference between the repository setting and an outdoor setting are significant. There is a dearth of relevant published studies that focus on evaporation rates from bare porous material, in an indoor (but ventilated) environment. Furthermore, our

system includes saturated brines, hygroscopic salt surfaces, and impurities that will be different from soil-water systems. Some preliminary laboratory and in-situ testing of evaporation from granular salt has been performed at WIPP and its associated surface laboratory (*Shawn Otto* and *Doug Weaver*, personal communication). In the in-situ experiments, environmental conditions were measured (temperature, relative humidity) with RoM salt was exposed to a ventilated environment while placed in pans or buckets on highly accurate scales. These experiments were terminated in February 2014.

Similarly, water vapor diffusion in soils has been studied by prior researchers (e.g., *Jin and Jury*, 1996; *Bruckler et al.*, 1989). The experiments typically measure diffusion through variably saturated materials and make comparisons with, e.g., the Millington-Quirk (*Millington and Quirk*, 1961) and other models for tortuosity. These experiments provide valuable insight into experimental design and setup, but have not been performed for material like RoM salt and with brine.

2. Methods

The experimental setup consisted of a 2 ft by 2 ft by 2 ft Plexiglas box, 0.5 in thick, with a removable lid, filled with granular salt. The setup is shown in Figure 2.

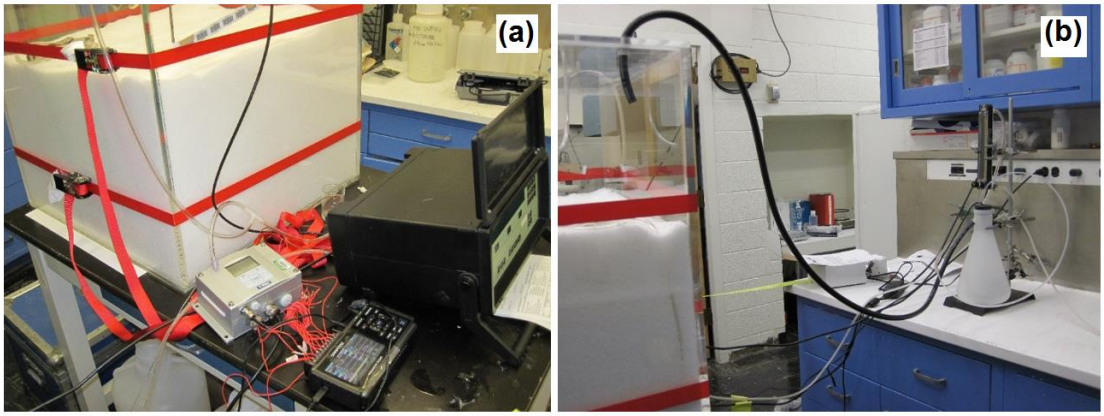

Figure 2: (a) Salt box, data loggers, and multi-gas monitor. (b) Setup showing the apparatus for airflow of known relative humidity (from the house air) through the beaker on the counter, monitored with a relative humidity sensor, through the lid of the box.

The material tested was store-bought granular salt of grain size 1-2 mm in diameter, with laboratory-measured unconsolidated porosity of $\phi \sim 45\%$ and bulk density of 1.2 g/mL. Bulk thermal conductivity is expected to vary with porosity and temperature (*Clayton and Gable*, 2009). An estimate for RoM salt at 25 and 250ºC is calculated based on the functions used in LANL porous flow simulator, FEHM (*Stauffer et al.*, 2013) which are derived from prior field experimental data. Table 1 lists properties of granular salt and bulk values. Bulk thermal conductivity and specific heat capacity are computed assuming a porosity of 45%. Use of the Kozeny-Carman equation (*Freeze and Cherry*, 1979) for spherical grains (porosity 45%) yields a permeability of $\sim 4 \times 10^{-9}$ m^2.

	Constant	Value	
Grain	Density, ρ (g/mL)[a]	2.2	
	Specific heat, c_p (J/kg-K)[b]	864	
	Thermal conductivity, K_t (W/m-K)[c]	25°C	250°C
		5.4	2.9
Bulk	Density, ρ (g/mL)[d]	1.2	
	Specific heat, c_p (J/kg-K)[e]	927	
	Thermal conductivity, K_t (W/m-K)[f]	25°C	250°C
		0.84	0.45

[a] *Eppelbaum et al*., 2014.
[b] *Domalski and Hearing*, 2014.
[c] Eq. 1 in *Stauffer et al*., 2013.
[d] Laboratory measurement.
[e] Bulk value based on porosity of 45%, $c_{p,bulk} = (1 - \phi)c_{p,salt} + \phi c_{p,air}$
[f] Eq. 2-4 in *Stauffer et al*., 2013, based on porosity of 45%.

Table 1: Properties of solid salt grains and bulk values.

The heater was a rectangular cartridge of size 2 in. width by 5 in. length by 2 in. height. Its temperature was controlled with a dedicated thermocouple in contact with the metal. Temperature in the salt was monitored using 20 thermocouples (24 in. Omega Engineering probes) hooked up to a Graphtec Midi Logger model GL220. They were lashed together with heat-resistant tape to make bundles that were placed 1, 3.25, and 6.75 in. laterally from the heater's edge (Figure 3). The thermocouple tips in each bundle were separated vertically by 2.25-3.5 in. to get point temperature measurements at 6 to 7 different depths in the salt. A Vaisala probe that monitored relative humidity and temperature with its own logger was located in the headspace of the box. The basic setup of the heater experiments is shown in Figure 4.

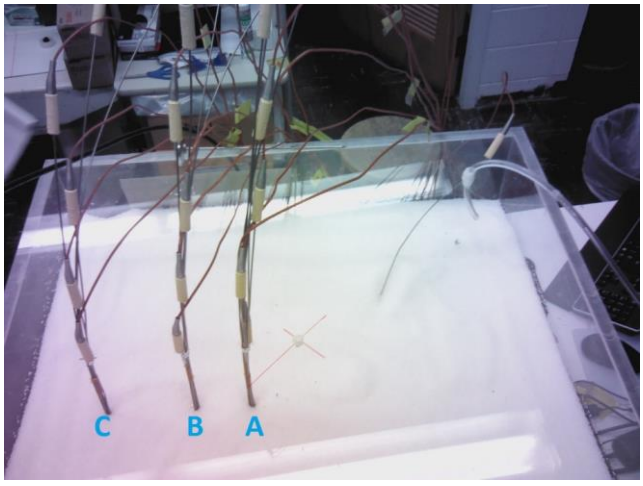

Figure 3. Location of thermocouple bundles. Bundle A is 1 in. from the heater's long edge; B is 3.25 in.; and C is 6.75 in.

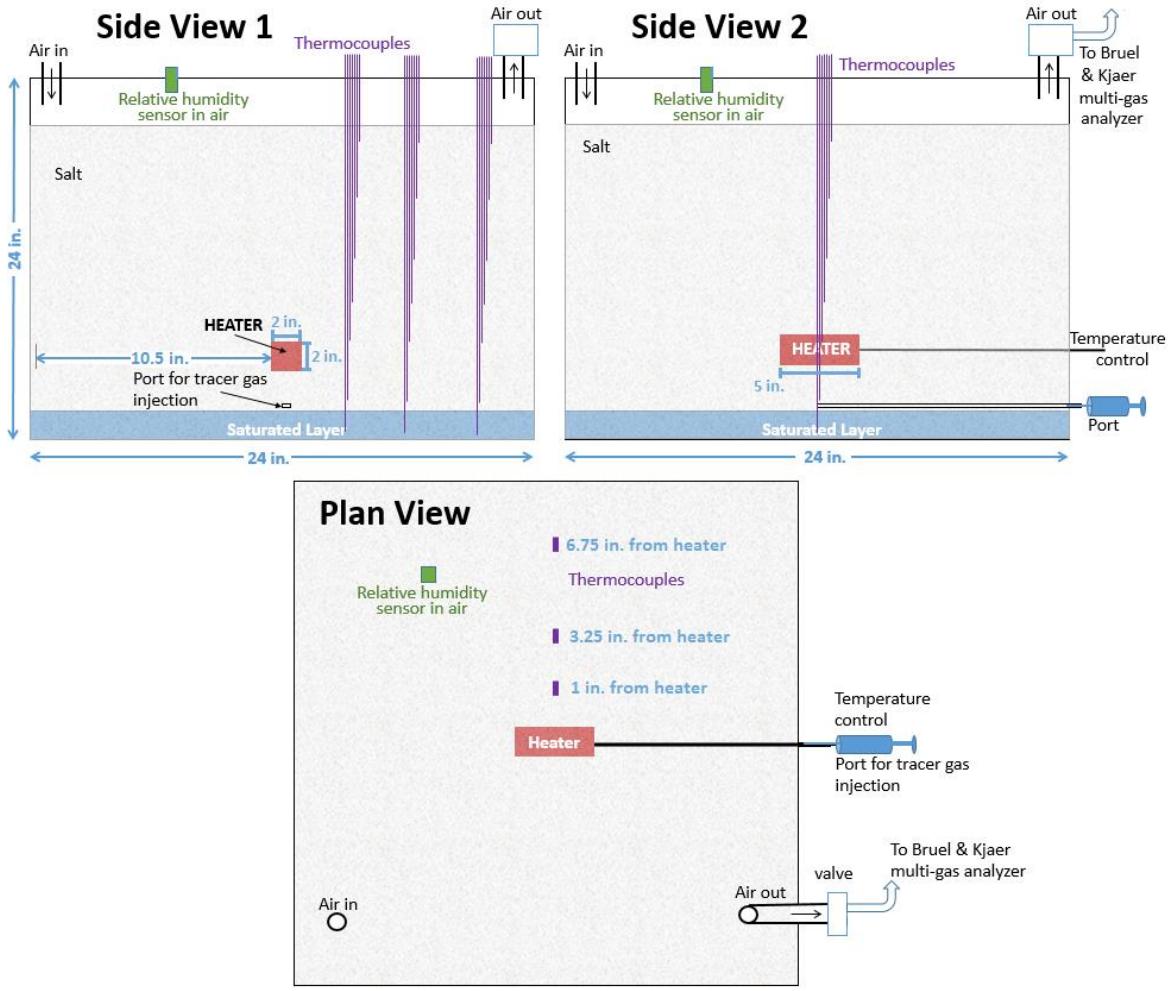

Figure 4. Schematic of the experimental setup. Some measurements are not indicated here because the placement of components varied between experiments.

Object	Dimensions/Location
Box	Outer dimensions L x W x H = 24 x 24 x 24 in. (including lid)
	Inner dimensions = 23.5 x 23.5 x 23.5 (excluding lid)
Heater	2 x 5 x 2 in.
Heater height	E1: 5.4 in. above ponded water; E2: 2.4 in.
Salt height	E1: 19.2 in. above box floor; E2: 16.7 in.
Ponded water	2.5 in. above box floor
Tracer injection port	2.8 in. above box floor, centered laterally in salt
Thermocouples	Bundle A = 1 in. from heater edge (narrow dimension) Bundle B = 3.25 in. from heater edge Bundle C = 6.75 in. from heater edge

Table 2. Dimensions and locations of apparatus in the salt laboratory experiments.

A ponded layer of saturated brine was present at the bottom of the salt, below the injection port. The ponded layer is not indented to mimic an expected feature of a typical bedded salt repository; it is used in these experiments to purposely provide a continual liquid source. The amount of water that flows to an excavated drift in salt is a highly uncertain quantity. Our experimental investigation is designed to study brine and water vapor movement in granular salt, recognizing that large uncertainties exist in the availability of mobile moisture in a typical generic bedded salt repository.

Table 3 lists the experiments performed to date under the scope of this work.

Test	**Analyses**
Experiment 0: Preliminary testing, unheated and heated	Airflow, relative humidity, temperature, gas tracer (chloroform), IR camera, pre-test porosity, post-test moisture content, post-test porosity and structure. Duration: 3 months.
Experiment 1: Heater test, with airflow	Relative humidity of headspace, temperature, gas tracers (chloroform and SF_6), IR camera, post-test porosity and structure, post-test moisture content.
Experiment 2: Heater test #2, with airflow	Relative humidity of headspace, temperature, gas tracers (chloroform and SF_6), IR camera.

Table 3. Experiment overview.

Prior to performing the main experiments (Experiment 1 and 2 in Table 3), the salt/brine/water vapor system was monitored and tested to help understand evaporation, water vapor diffusion, and porosity/structural change of the granular salt (Experiment 0). During testing, 3 L saturated brine was injected at the bottom of the box and the headspace was monitored for relative humidity. For several weeks, airflow was first circulated, then shut off, and then turned back on (repeatedly) to see the equilibration and re-equilibration of relative humidity in the air space. The house air in was monitored, but not controlled, for temperature and relative humidity. The airflow rate was tested with a gas injection of chloroform in the headspace and measured with a flow meter. Chloroform was also injected at the bottom of the box and monitored above the salt to test the equipment and observed breakthrough.

During Experiment 0, the heater was installed near the top of the box and tested for function and temperature distribution. The heater ran at 250ºC for 24 hours. The box was allowed to cool and was sampled for porosity and moisture distribution. Post-test forensics consisted of digging back into the box and noting regions of structural change, e.g., consolidation, and sending samples to be made into thin sections.

Experiments 1 and 2 were run with the heater placed deep in the box, above the level of ponded brine, with regular tracer injections in the salt near the bottom of the box. In Experiment 1, the heater was 14 cm (5.4 in.) above the water level; in experiment 2, it was closer to the water at 6 cm (2.4 in.). For Experiment 1 the box was filled with 450 lbs fresh granular salt (to height 19.2 in.) and 10 L saturated brine were added to the bottom, resulting in a ponded water depth of 2.5 in. In Experiment 2, 400 lbs salt was used with a height of 16.7 cm and ponded water depth of 2.5 in. In Experiment 1, airflow was measured at 1.053 L/min (63,180 cm^3/hr) or 1.9 air turnovers per hour in the headspace. For Experiment 2, airflow was lower at 0.702 L/min

(42,120 cm^3/hr) and the volume was greater, leading to a lower air turnover rate of approximately 0.65 cm^3/hr.

The injection port for tracer gases consists of a thin stainless steel tube from the edge to the middle of the box, above the ponded water line and below the heater (Figure 5). The port has a septum for gas injection by syringe. The tracer gases–chloroform ($CHCl_3$) and SF_6–were chosen because a Bruel & Kjaer photo-acoustic multi-gas monitor was made available. (The instrument can measure those two gases plus trichloroethylene, tetrachloroethylene, acetone, and water vapor.) SF_6 was chosen for its conservative (negligibly partitioning) behavior; chloroform was chosen for comparison (using a gas tracer with non-negligible Henry's Law partitioning produces additional information). Initially, chloroform alone was used as the tracer gas; the procedure was vaporizing 0.1 mL liquid chloroform under an applied vacuum. Subsequent tests used both chloroform and SF_6, which were pre-mixed in a syringe. The tracer pulse was injected quickly.

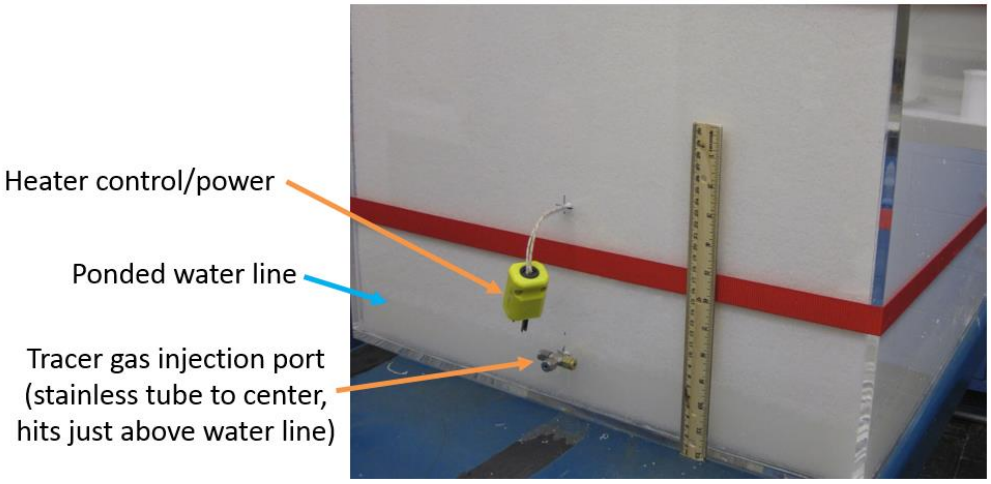

Figure 5. Experiment 1 setup showing heater controller, injection port, and ponded water line. A slight rise in the injection port stainless steel tube keeps it above the ponded water line.

An infrared (IR) camera (FlirT-640, fully calibrated) was used to measure temperature on the outer face of the Plexiglas box. Its temperature sensitivity is <0.02ºC at 30ºC (*Hank Herber*, personal communication).

Following cessation of heating and several weeks of sitting without airflow, the box was excavated in Experiment 1. Samples were collected for moisture content and thin section.

A timeline of events for Experiment 1 is provided in Table 4. A timeline for Experiment 2 is presented in Table 5.

Date	Action
4/20/15–4/21/15	Box setup: salt placed in box; heater enclosed in salt with controlling thermocouple; gas tracer port installed; 10 L saturated brine added to bottom of box (during salt emplacement); holes drilled in lid for thermocouple bundles; thermocouples placed in salt; relative humidity data collection begins
4/22/15, 9:51 am–5:06 pm	Pre-test chloroform injection run (T1-cool)
4/23/15, 9:43 am 4/23/15, 12:10 pm 4/23/15, 5:17 pm	Heater set to 160°C Heater temperature raised to 200°C Heater temperature raised to 260°C
4/27/15, 9:56 am–2:25 pm	Chloroform injection run (T2-hot)
4/30/15, 9:48 am–2:17 pm	Chloroform injection run (T3-hot)
5/7/15, 12:01 pm–5:11 pm	Chloroform/SF_6 injection run (T4-hot)
5/8/15, 12:15 pm	Heater turned off
5/11/15, 12:17 pm–6:13 pm	Post-test chloroform/SF_6 injection run (T5-cool)
6/16/15–6/17/15	Destructive post-test forensics

Table 4. Timeline of events for Experiment 1.

Date	Action
7/10-11/15	Box setup: salt placed in box; heater enclosed in salt with controlling thermocouple; 9 L saturated brine added to bottom of box (during salt emplacement); relative humidity data collection begins in air space
7/13-15/15	Thermocouple emplacement
7/15/15, 9:40 am–2:15 pm	First cool pre-test tracer test (poor data)
7/16/15, 8:35 am–4:25 pm	Duplicate cool pre-test tracer (T2-1-cool)
7/17/15, 8:15 am	Heater turned to 155°C
7/17/15, 10:25 am	Heater turned to 200°C
7/17/15, 11:49 am–3:36 pm	Heated tracer test (T2-2-hot)
7/20/15, 8:17 am–10:45 am	Attempted tracer test (poor data)
7/21/15, 8:35 am	Heater turned off
7/22/15, 8:58 am	Airflow turned off

Table 5. Timeline of events for Experiment 2.

3. Results and Discussion

The following sections describe experimental results from the preliminary testing (Experiment 0), the first full test run (Experiment 1), and Experiment 2.

3.1 Temperature Distribution

Temperatures in the heated experiments in granular salt were generally lower than cursory pre-test numerical modeling (*Jordan et al.*, 2014) indicated. The time series of temperature for several thermocouples in Experiment 1 is shown in Figure 6, showing the staged temperature increases of the heater during the first day and the approach to steady-state. At thermocouple A4, the closest one to the heater (3.2 cm away), the timescale for conductive equilibration ($\sim L^2/D_T$, where $D_T = K_t/\rho c_p$) is approximately 42 minutes based on the bulk thermal properties of salt (Table 1). This is slightly faster than the times seen in Figure 6(b) for thermocouple A4's temperatures to approach their equilibrium values (~2 hours) after *each* temperature jump. Inaccuracies in the thermal properties or simplifications made for bulk calculations may be responsible for the discrepancy.

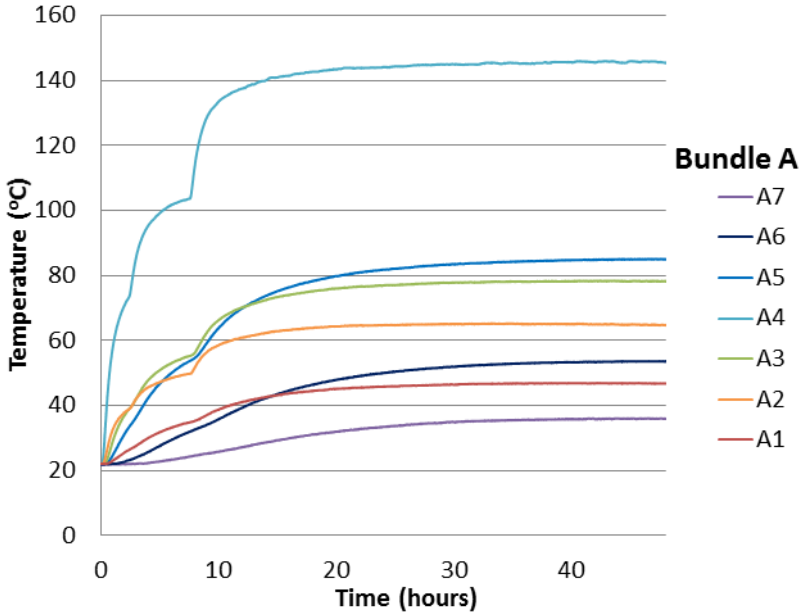

Figure 6. Temperature with time for the thermocouples of bundle A (closest to heater). Thermocouple A7 is the shallowest in the salt and A1 is the deepest. Heater temperature is 260ºC.

Figure 7 shows the steady-state temperature with depth in the box for Experiments 1 and 2. The heater temperature and depth and depth of the ponded water line are indicated. The striking result that the temperature gradient is much flatter in Experiment 2 (more similar temperatures) throughout the box, particularly at points 2 and 3, may be evidence for heat pipe activity (*Birkholzer et al.*, 2004) compared to Experiment 1. The other feature consistent with heat pipe activity is the hotter temperatures at Bundle C for Experiment 2. While the heater is 60ºC cooler in Experiment 2, at a distance of 6.75 in laterally from the heater, temperatures are nearly 15ºC hotter. This type of behavior is seen in simulations with heat pipe activity when comparing temperatures close to the heat source (generally cooler) with those further away (generally hotter) (*Jordan et al.*, 2015).

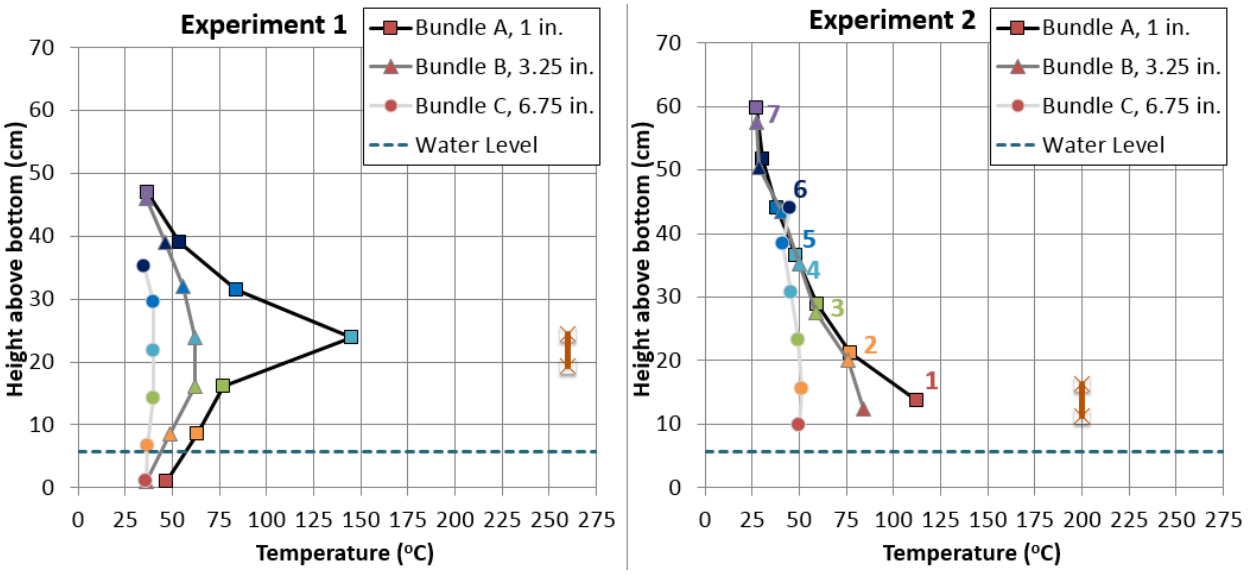

Figure 7. Steady-state temperature distribution with depth for Experiments 1 and 2. The distance from the thermocouple bundle to the heater is indicated.

The IR camera showed similar effects between the two experiments. While it is difficult to get a square face-on picture of the side of the apparatus due to limited space in the lab as well as reflection issues with the infrared imagery, the temperature-calibrated IR images of the Plexiglas faces will still be useful for constraining the numerical models. Figure 8 shows two faces of the box in Experiment 1, with (a) showing the side parallel to the long edge of the heater; the picture was taken 11 days after heater initiation.

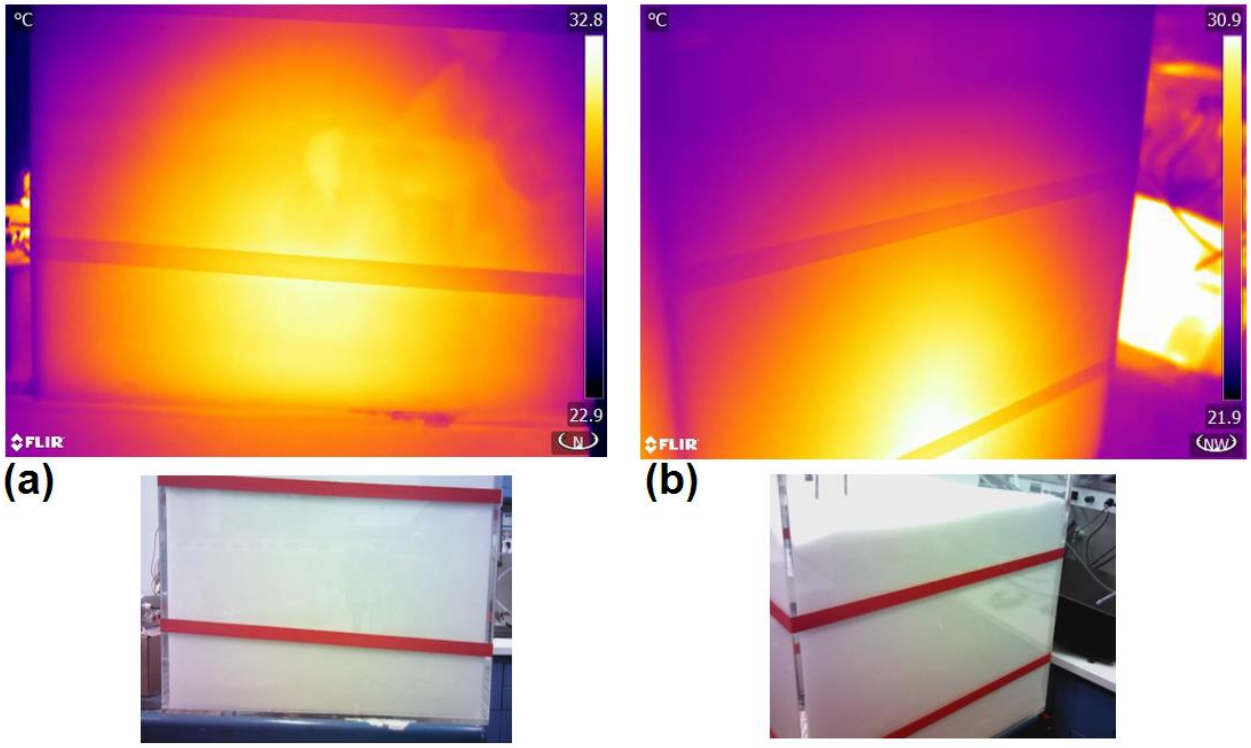

Figure 8. Infrared images taken 5/4/15 (Experiment 1) of (a) the salt box face parallel to the long edge (5") of the heater and (b) parallel to the short edge (2") of the heater. Photos courtesy of Hank Herber.

Figure 9 shows the temperature of the same face shown in Figure 8(a) for Experiment 2. The results confirm the hotter temperatures far from the heat source seen in the thermocouple data, with a maximum temperature on the Plexiglas face of 37.1°C, compared to 32.8°C in Experiment 1.

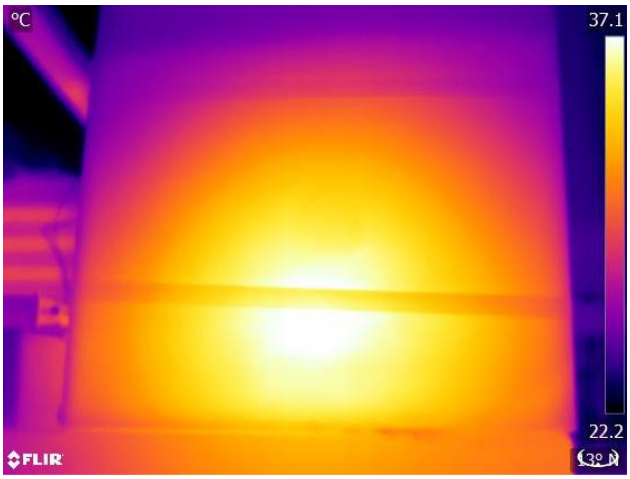

Figure 9. Infrared images taken 7/21/15 (Experiment 2) of the salt box face parallel to the long edge of the heater, as in Figure 8(a). Photo courtesy of Hank Herber.

3.2 Tracer Tests

One tracer test was performed during preliminary testing of the box and equipment (Experiment 0) and five tracer tests were performed during Experiment 1. Two tracer tests were performed in Experiment 2 before the injection port became fully clogged.

Multiple strongly coupled processes that affect gas migration through the variable porosity of the salt box experiment make a simplified analytical or numerical modeling approach quite challenging. Numerical simulation of the experiment is optimal to fully analyze the parameters and processes (e.g., changing tortuosity, tracer mass recovery). Fully coupled thermal/hydrological/chemical modeling is planned. On the other hand, an approach to fitting the breakthrough curves with a particular solution to a highly idealized case of the advection-dispersion equation was found to be useful for providing intuition about the observed laboratory data. The fitted curves do not provide accurate values of effective tortuosity, vertical velocity, or total mass recovered from the system due to the simplifications and unrealistic assumptions that must be made. However, when comparing like curves from equivalent scenarios to each other, changes in the fitted parameters can show the timing and suggest the nature of internal structural change.

Figure 10 shows a schematic of the processes present and the idealized conceptual model of the system. A discussion of the major assumptions and approximations required for this model is given below.

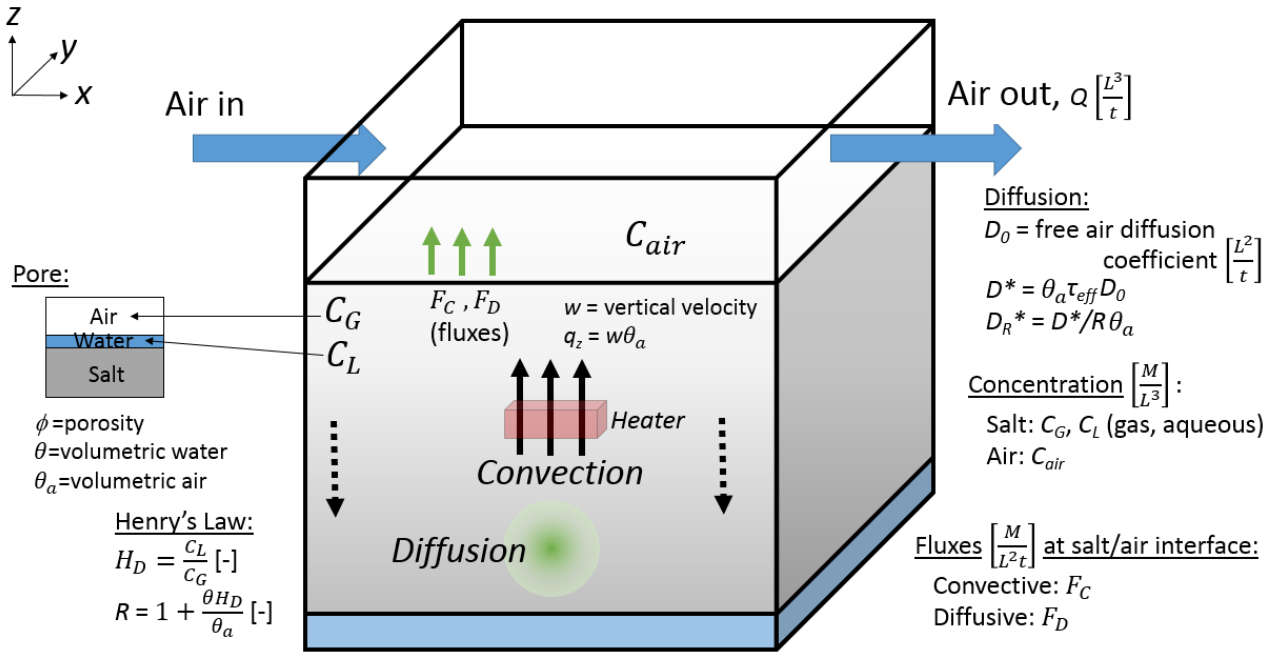

Figure 10. Conceptual diagram of the tracer transport model. Downward flow (dashed arrows) is not modeled.

The breakthrough tracer gas data were fit by an analytical solution to the 3-D advection-dispersion equation with one-dimensional (vertical) flow, homogeneous and isotropic diffusivity, and a retardation factor due to Henry's Law partitioning of chloroform into the aqueous phase (where the aqueous phase tracer is assumed immobile):

$$\frac{\partial C_G}{\partial t} = D_R^* \nabla^2 C_G - w_R \frac{\partial C_G}{\partial z}, \quad (1)$$

where C_G is the gas phase concentration; $D_R^* = D^* \theta_a^{-1} R^{-1}$ is the retardation dispersion coefficient, with R as the retardation factor due to Henry's Law partitioning and $D^* = \theta_a \tau_{eff} D_0$, where τ_{eff} is an effective tortuosity and D^* is assumed to include any effects of dispersion for the heated cases; w is the vertical absolute velocity ($w = q_z/\theta_a$) and $w_R = w/R$. Additional related variables are shown in Figure 10. The retardation factor is calculated by

$$R = 1 + \theta H_d/\theta_a \quad (2)$$

where θ is the volumetric water content, θ_a is the volumetric air content, and H_d is a dimensionless Henry's Law partitioning coefficient of the form $H_d = C_L/C_G$.

A discussion of the major assumptions and approximations required for this model is given below. Assuming infinite 3-D Cartesian geometry and a pulse input of total mass M at $t = 0$ (ignoring residual tracer concentrations from previous tests), an analytical solution for concentration at location (x, y, z) and time t is given by (*Hemond and Fechner*, 1999, with modifications for unsaturated media and retardation):

$$C_G = \frac{M}{8\theta_a \pi^{3/2} t^{3/2} \sqrt{D_R^{*3}}} \exp\left[-\frac{1}{4 D_R^* t} \left(x^2 + y^2 + (z - w_R t)^2 \right) \right] \quad (3)$$

As an example, Figure 11 shows concentrations at $t = 5$ hours across the x, y top surface of the salt at $z = 42$ cm based on Equation 3 for SF_6 with $\tau_{eff} = 0.26$, $\theta_a = 0.45$, $w = 0.0023$ cm/s, $R = 1$.

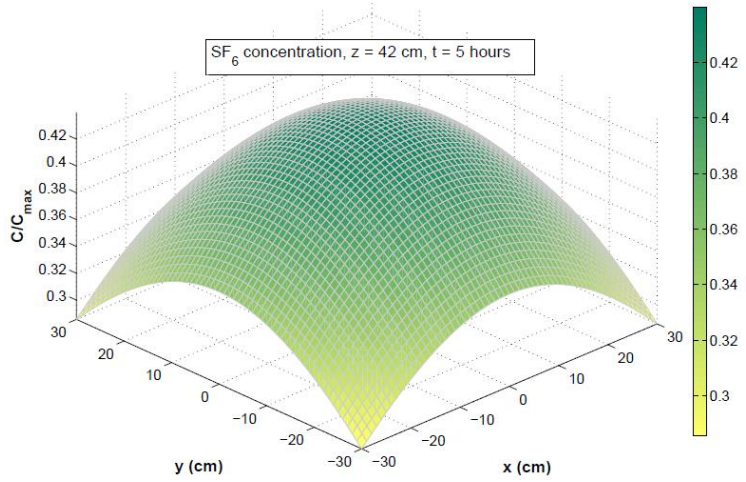

Figure 11. Analytical solution (equation 3) for gas phase concentration of SF_6 in the salt at $z = 42$ cm, $t = 5$ hours, normalized by peak concentration.

However, because this solution assumes an infinite homogeneous porous material, an additional approximation is made to handle the more realistic boundary condition of ventilated air space above the salt and flux-averaged concentrations sampled from that space. That is, we seek C_{air}, the concentration in the mixed, ventilated volume of air (V = 33,000 cm^3; volumetric air flow rate Q = 65,000 cm^3/hr). Figure 12 shows a schematic of the air mixing model discussed below.

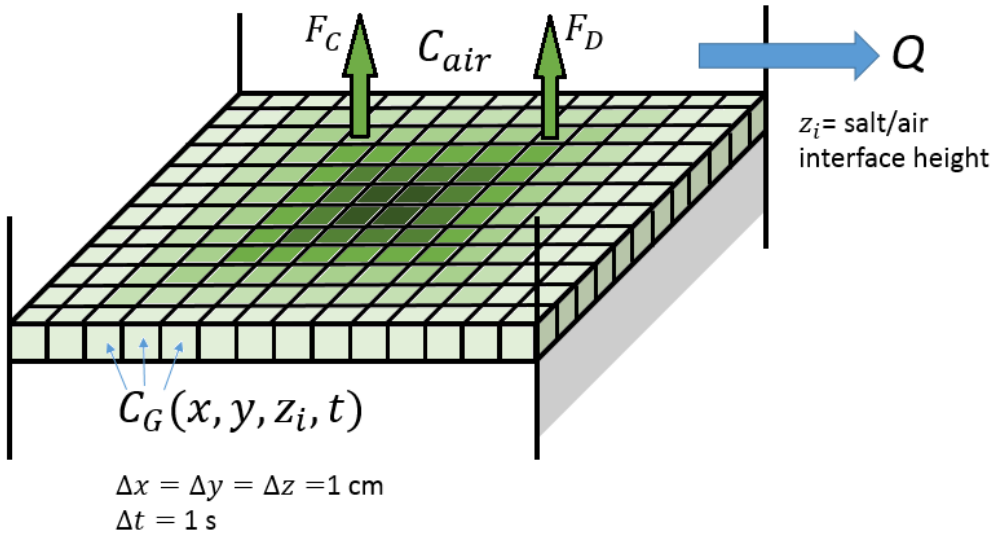

Figure 12. Schematic of the air mixing model.

The first iteration of the air mixing model assumed perfect evacuation of the airspace on each timestep, i.e., zero concentration in the air was used to calculate the diffusive flux based on concentration gradient from the top of the salt to the air and to mix with the diffusive and convective fluxes. However, this is inaccurate because the turnover rate in the air was ~2 air space volumes per hour, while sampling was performed every few minutes. An improved version of the model used the known flow rate to adjust the concentration of the air instead of assuming zero concentrations.

This model predicts breakthrough concentrations as follows. The pore gas concentration (C_G) is first calculated for all time and x, y at z = 42 cm (the top of the salt) using Equation 3. Next, the air space is considered well-mixed and fluxes from convection (F_C) and diffusion (F_D) are calculated across the porous salt/free air interface:

$$F_C = wC_G$$
$$F_D = -\theta_a D_0 \frac{dC}{dz} \quad (4)$$

Where $\theta_a D_0$ is used instead of D_{eff} to represent the boundary between the salt and the free air (an approximation). The problem is discretized into 1 cm “cells” throughout the domain, where

$dC \approx C_G - C_{air}$ and $dz = \Delta z = 1$ cm. At each timestep, to compute the diffusive flux, C_{air} from the previous timestep is used. The discretized fluxes are multiplied by cell area and summed across the entire salt/air interface to obtain the mass into the air in time dt. The mass flow rate out of the air space is computed as $C_{air}Q$, where Q is the volumetric rate of airflow and C_{air} from the previous timestep is used. Multiplied by time dt, the change in mass in the air in each timestep dM_{air} is

$$dM_{air} = \left(\sum_x \sum_y (F_C + F_D) dx\, dy \right) dt - Q C_{air} dt \tag{5}$$

The total mass in the air, M_{air}, at any time t is the sum of the change in mass during that timestep and the previous timestep mass; dividing by volume provides the air space concentration at each timestep:

$$C_{air}(t + dt) = \frac{M_{air}(t) + dM_{air}}{V} \tag{6}$$

This is our approximate model for fitting the measured concentrations in the air space. Where C_{air} is required to compute the desired quantities at time $t + dt$, the known value at time t is used in a timestepping loop.

The free-air diffusivity, D_0, and Henry's Law coefficient, H_d, of the tracers depend on temperature. The model assumes a single value of D_0 and H_d across the domain, which is an inaccurate assumption while a heterogeneous temperature field is established during heating; both are strongly dependent on temperature. For "cool" cases (unheated), D_0 and H_d at 25°C are used. For "hot" cases (during heating), values at 75°C are used. Figure 13(a) shows H_d versus temperature for chloroform. SF_6 is considerably more conservative as a gas-phase tracer, with $H_d = 5.6 \times 10^{-3}$ at 25°C, and is not shown. Figure 13(b) shows D_0 as a function of temperature for chloroform and SF_6.

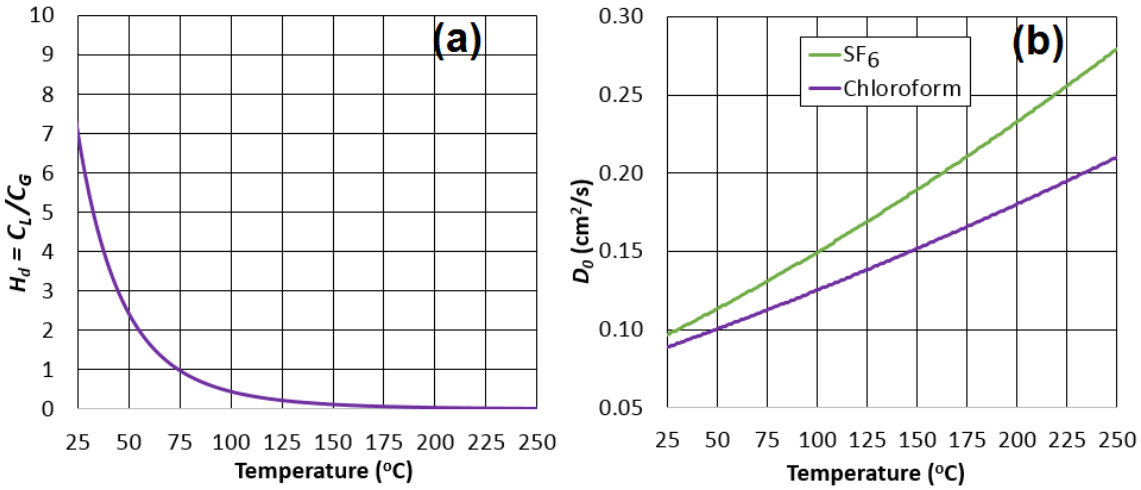

Figure 13. (a) Chloroform dimensionless Henry's Law coefficient, $H_d = C_L/C_G$, as a function of temperature (*Sander*, 2015). (b) Free-air diffusion coefficient of SF_6 (*Watts*, 1971) and chloroform (*Marrero and Mason*, 1972) as a function of temperature.

Constant		**Value**	
Porosity, ϕ		0.45	
Saturation, S		0.01	
Salt depth, z (cm)		42	
Airspace volume, V (cm^3)		3.3×10^4	
Volumetric air flow rate, Q (cm^3/hr)		6.5×10^4	
Free-air diffusivity, D_0 (cm^2/s)		25ºC	75ºC
	Chloroform	0.0866	0.113
	SF_6	0.0968	0.131
Henry's Law coefficient, H_d (C_L/C_G)		25ºC	75ºC
	Chloroform	1.07	1.01
	SF_6	-	-

Table 6: Breakthrough curve fitting model parameters.

A schematic of the tracer tests for Experiment 1 is presented in Figure 14. The hypothesis or anticipated result is that the altered interior structure between the pre- and post-heating tracer runs will lead to a noticeable change in the breakthrough curves. Note that the actual distribution of porosity after heating, as shown in Figure 14 in a pattern that resembles pre-experiment numerical modeling, is unknown until post-test forensics and porosity sampling (section 3.3). The fitted parameters in the model are τ_{eff}, $w = w_R R$, and M (when applicable), despite considerable uncertainties in other parameters such as porosity (set to $\phi = 0.45$), saturation (assumed liquid saturation of $S = 0.01$ or $\theta_a = \phi[1 - S] = 0.446$), and temperature-dependent free air diffusivity and Henry's Law parameters (see discussion of assumptions below).

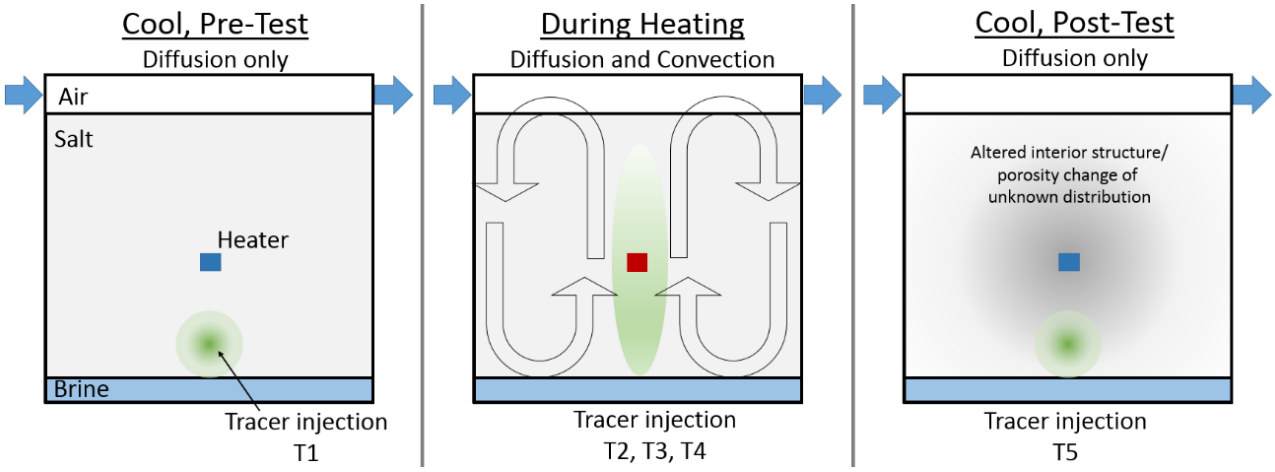

Figure 14. Schematic of tracer tests performed during Experiment 1. Note that the interior structure depicted in the post-test scenario is for illustration only and is not intended to be representative of the observed porosity distribution.

The following discussion presents the tracer gas data from Experiment 1 and model fitting results. The data come from the five tracer runs (T1 through T5) described in Table 4. The results for Experiment 2 are presented after the full discussion of Experiment 1.

Figure 15 shows the first three chloroform breakthrough curves for Experiment 1 (T1-cool, T2-hot, and T3-hot). For these three tracer tests, the same quantity of chloroform was injected (0.1 mL; 149 mg). The modeled curves are also shown. The best fit to the model curves came from the first iteration of the mixing model, where C_{air} was assumed perfectly evacuated, despite the presumed more realistic assumptions in the second iteration. All breakthrough curves shown below are from this model. A full discussion of assumptions and sources of error in the simplified models is presented below.

To fit the cool, pre-heating case (T1 on 4/22/15), a τ_{eff} of 0.61 provides an excellent match to the data with diffusion only and no convection ($w = 0$). Although this value agrees well with other published values for tortuosity, e.g., $\tau \sim 0.66$ (*Jury and Horton*, 2004), we stress that the fitted parameters to this highly idealized model are not expected to be realistic; they are used for comparison of otherwise similar scenarios (see below) and are used to gain intuition into the processes (advection, diffusion, dispersion) operating in the experimental apparatus.

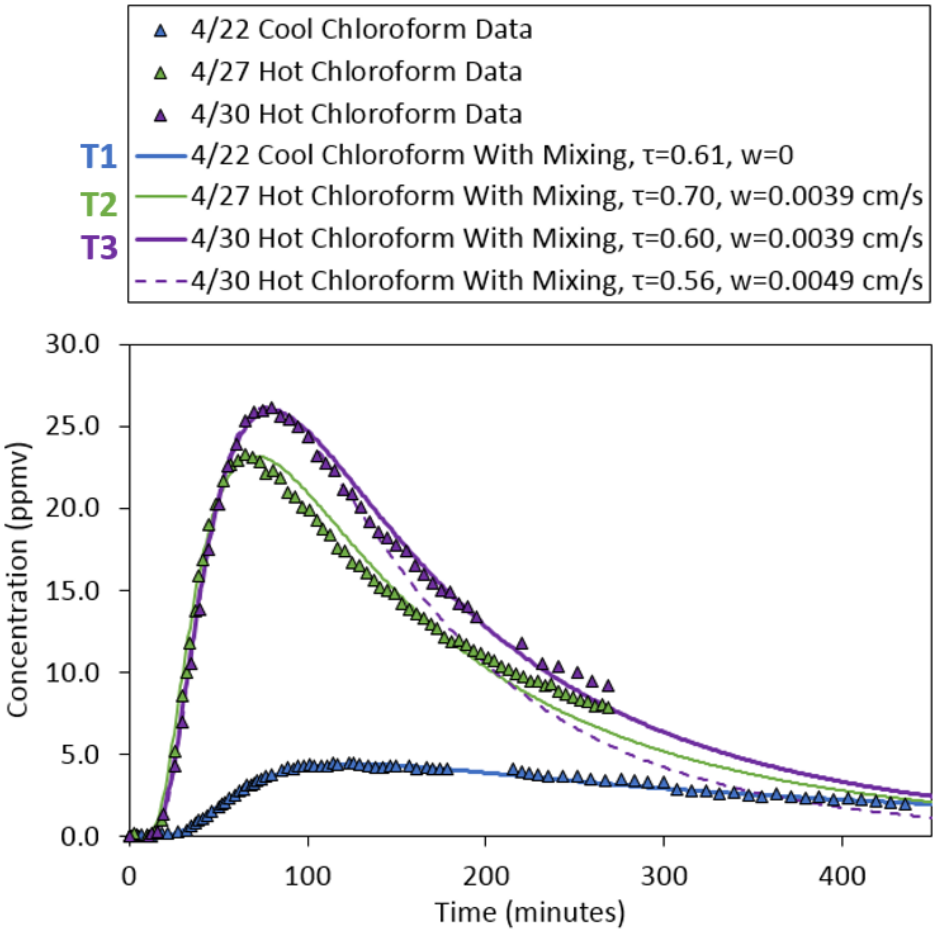

Figure 15. Chloroform breakthrough curves, both data and modeled, for the pre-test cool tracer run (T1-cool on 4/22/15), and the first and second heated tracer tests (T2-hot on 4/27/15 and T3-hot on 4/30/15).

While the air mixing model matches the data extremely well for the cool case, the modeled curves perform worse for the heated tracer tests, especially in the tail (potentially due to residual concentrations from previous tests or other effects; assumptions are discussed below). A key observation, nonetheless, is that convective velocity (w) is *required* to fit the hot breakthrough curves. That is, the data cannot be matched by changing "effective" tortuosity alone. The best-fit vertical velocities of ~0.004 cm/s within the salt (height z = 42 cm) with D_0 at 75°C = 0.11 cm^2/s produce a Peclet number of Pe = wz/D_0 ~ 1.5, suggesting neither advective nor diffusive dominance in this system.

A jump occurs between the cool, pre-test effective tortuosity (τ_{eff} = 0.61) and the first heated test (τ_{eff} = 0.70), but this does not likely represent a physical change in the salt but instead other factors such as dispersivity as well as assumptions and issues with the model when convective fluxes are also present (see discussion below about simplifications). For the results that follow, we will generally compare cool cases directly to each other (pre- and post-heating; T1 and T5) and hot cases directly to each other (T2, T3, T4) to observe the differences that occur for cases that are otherwise comparable.

The best fit values of M for the simplified mixing model were generally too high compared to the actual injected mass by a factor of ~10 based on 0.1 mL chloroform (0.149 g) injected. However, the second iteration of the mixing model produced M of a much more reasonable 80% of actual injected mass for the *hot* cases. The *cool* case has significantly lower recovery than the two hot cases with 0.1 mL injected (40%). Henry's Law partitioning, where more tracer dissolves into the aqueous phase for the cool case, may be responsible for some of the loss. There may also be extra condensation of chloroform for the cool case. Other assumptions and errors in the model that may contribute to these low recovery factors (e.g., infinite domain) are discussed below.

For the discussion that follows, the curves and model fits have been normalized by C/C_{max}. We will be comparing fitted parameters τ_{eff} and w, which do not change when scaled from actual to normalized concentrations. Figure 16 shows pre- and post-heating chloroform breakthrough curves in the air space for Experiment 1 (T1, 4/22/15; and T5, 5/11/15), normalized by maximum detected chloroform (C_{max}) and compared to the normalized solution based on the air mixing model.

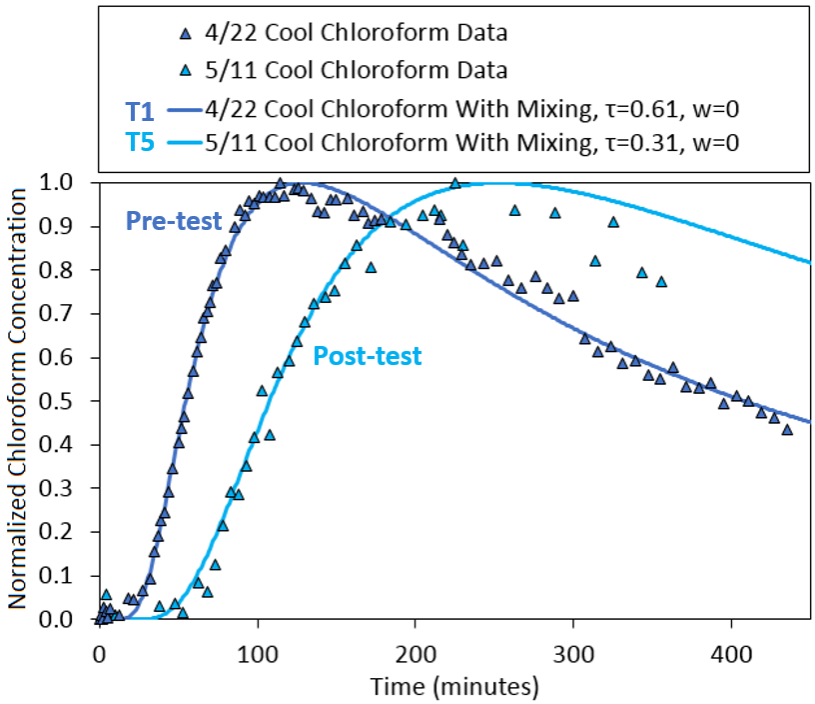

Figure 16. Chloroform breakthrough curves, both data and modeled, for the pre-test cool tracer run (T1-cool on 4/22/15) and final post-test cool run (T5-cool on 5/11/15).

The cool, pre- and post-test chloroform breakthrough curves differ substantially in the effective tortuosity required to fit the data (τ_{eff} = 0.61 to 0.31). We propose that this is due to structural changes in the salt box throughout the heating and concurrent moisture movement. (Observed structural changes after the box was excavated are discussed in section 3.3.)

The decrease in τ_{eff} over time during the weeks of heating is also evident in the heated breakthrough curves (Figure 17). In particular, it seems that a fairly consistent trend of decreasing τ_{eff} between the first two heated tests (three days apart) and the last (seven days later) takes place. The best-fit values of τ_{eff} go from 0.70 (4/27; T2) to 0.60 (4/30; T3) to 0.34 (5/07; T4). Best-fit values of *w* are also presented. The first two breakthrough curves, as discussed above, are not particularly well fit in the tail. The third breakthrough curve (5/07) can be very well matched by the model but at a velocity that diverges from the other two. We note that the post-test cool (diffusion only) model for both chloroform and SF_6 (discussed below) is a worse match to the model than the pre-test, presumably much more homogeneous case. More likely than a change in velocity (the system is at steady-state temperature) is a change in structure that makes the model assumptions even more challenged. Therefore, although the third tracer test appears to match the data for the hot cases much better than the first two, it is likely a coincidence. If the velocity is the same as the fitted value for the heated cases, an even lower τ_{eff} is required to fit the data (~0.29) but the fit performs poorly in the tail (not shown).

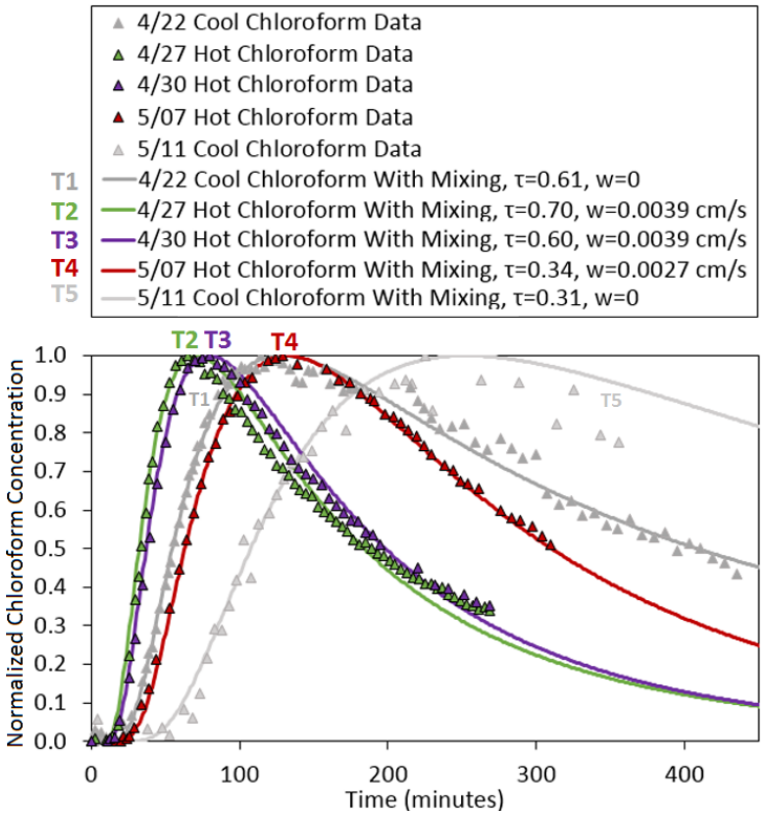

Figure 17. Chloroform breakthrough curves, both data and modeled, for the heated cases (T2-hot on 4/27/15; T3-hot on 4/30/15; and T4-hot on 5/07/15). The cool cases of Figure 16 (T1, pre-test and T2, post-test) are shown in gray for comparison.

Figure 18 compares chloroform breakthrough curves shown above with SF_6 data from the same runs (SF_6 was only included in the final two tests, T4-hot and T5-cool). First, we note that very similar values of effective tortuosity are obtained for the two tracers, indicating that the model's handling of Henry's law partitioning–which imparts a retardation factor for chloroform, particularly during the cool test–is working. The differences in the hot chloroform and SF_6 curves are due almost entirely to the different diffusivities between the two gases (SF_6 is more diffusive). On the other hand, less than half the difference between the cool curves can be explained by their diffusivities while the rest is due to partitioning of the vapor into the aqueous phase. This clearly demonstrates the strong temperature dependency of Henry's Law partitioning.

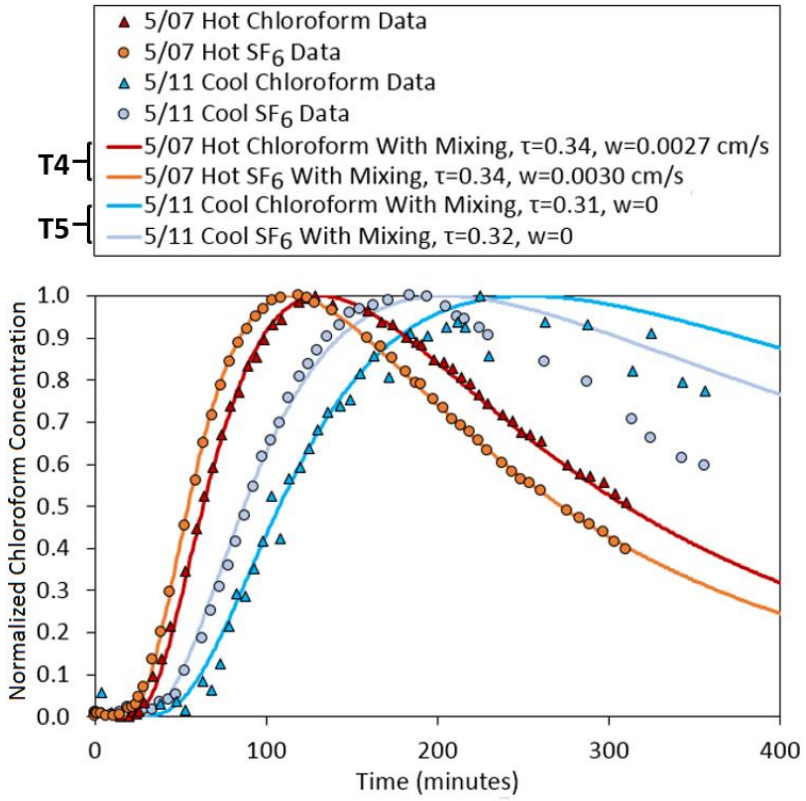

Figure 18. Chloroform and SF_6 breakthrough curves, both data and modeled, for T4-hot on 5/07/15 and T5-cool on 5/11/15.

The heated case best-fit vertical velocity of ~0.0030 cm/s for SF_6 (D_0 at 75°C = 0.13 cm^2/s) produces a Pe ~ 0.97; for chloroform with w = 0.0027 cm/s and D_0 at 75°C = 0.11 cm^2/s, Pe ~ 1.0. Table 7 summarizes the best-fit results for tracer tests T1 to T5.

Test	Date	Tracer	τ_{eff}	w (cm/s)	Pe
T1 (cool)	4/22/2015	Chloroform	0.61	0	*N/A*
T2 (hot)	4/27/2015	Chloroform	0.70	0.0039	1.49
T3 (hot)	4/30/2015	Chloroform	0.60	0.0039	1.49
T4 (hot)	5/7/2015	Chloroform	0.34	0.0027	1.03
		SF_6	0.34	0.0030	0.97
T5 (cool)	5/11/2015	Chloroform	0.31	0	*N/A*
		SF_6	0.32	0	*N/A*

Table 7. Summary of results from the best fits to the tracer breakthrough model.

Experiment 2 was intended to verify the results from Experiment 1 with a change to the configuration (lower heater, lower temperature). However, the injection port became clogged after the first heated test and subsequent tests could not be performed (e.g., post-test breakthrough). The first two sets of good data (T2-1, cool and T2-2, hot) are presented in Figure 19. Fitted effective tortuosities are slightly lower than those for T1 and T2 in Experiment 1. As before, a jump in τ_{eff} for heated cases compared to cool is observed, potentially as a result of dispersion. The model fits the heated case extremely well, but the cool analytical solution behaves poorly in the tail. Assumptions and approximations that would lead to such poorly fitting behavior are discussed below.

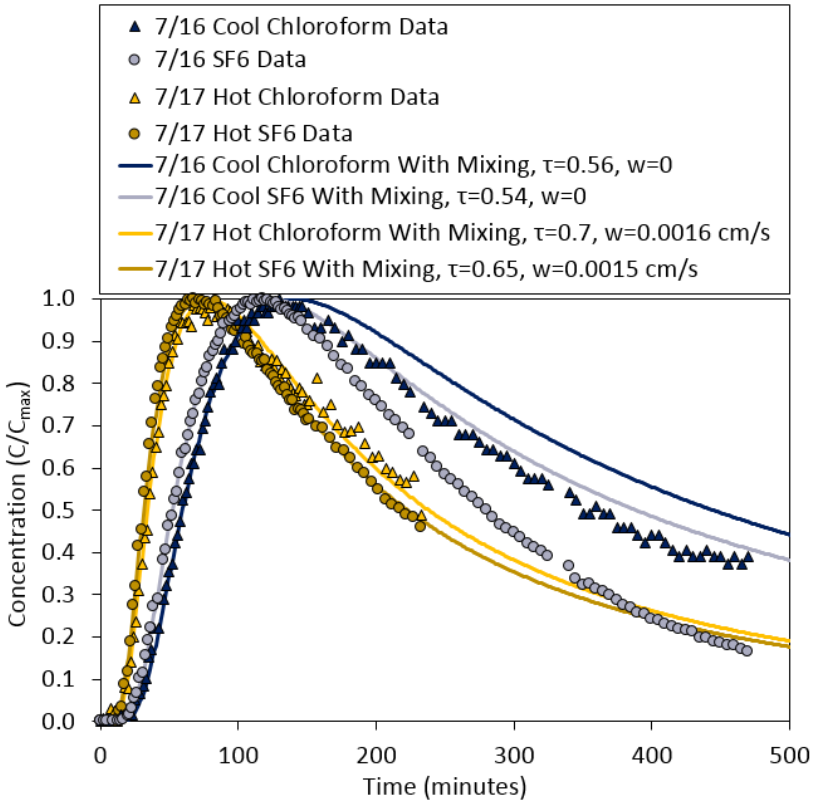

Figure 19. Chloroform and SF_6 breakthrough curves, both data and modeled, for T2-1-cool on 7/16/15 and T2-2-hot on 7/17/15.

There are abundant issues and assumptions with our model; however, even without the model, the data show a clear trend towards delayed breakthrough over time in Experiment 1 and the model provides intuition and supports the argument that structural change is the cause. While various models were developed over the course of analyzing these data, from a clearly inaccurate resident concentration-type model to the various iterations of the air-mixing model, the primary results remained unchanged throughout (while values of the best-fit parameters varied): (1) that effective tortuosity declines from the pre-test to the post-test tracer runs, as well as during the heated runs; (2) that some sort of convective velocity parameter is required to fit the hot cases compared to the cool cases; and also that Henry's law partitioning explains well the differences in chloroform and SF_6 breakthrough. Simplifications, assumptions, and issues in the model are discussed in the following paragraphs.

The analytical solution for C_G (Equation 3) assumes infinite 3-D space, despite being applied to a finite box. The box would be better modeled as a finite domain. The bottom boundary is a declining layer of ponded water; while it would be simple for the diffusion-only case to assume the water is a no-flow boundary, in fact there is some (increasing with time) available pore space below the injection port for filtering of the tracer gas, as well as partitioning into the water (for chloroform). At the air/salt interface, the solution for C_G without consideration of the actual boundary is applied and then modified by the air mixing model, instead of more accurately representing the boundary as part of a finite domain with an air mixing model. The presence of a boundary layer at the salt-air interface makes this assumption more realistic, but still concentrations at depth will be modified by the fresher air above.

Another simplification is that only an upward z-component of velocity is considered. Although we expect downward replenishment at the edges of the box of the central column of rising air above the heater, this is not included in either the computation of C_G nor the air mixing model. This assumption is made because the downward component at the edges affects the lower-concentration regions of the box, while the higher-concentration regions are subject to the upward velocity component at the center.

Most of the curves in this analysis show C/C_{max}, instead of using a known C_0 or injected mass (M). While the relative peaks and integrated mass of the curves provide additional information about tracer transport and storage, they do not affect the fitted w and τ_{eff} parameters but merely scale the solution by a multiplier. It does not affect the primary conclusions of this work (section 4). In future work, attention will be paid to injected mass/concentration and additional analysis can be performed. Curves from the first three runs had the same M chloroform injected, but the last two runs followed a different procedure when SF_6 was added to make a mixed tracer. In the future, all runs will use the same injected mass.

Other assumptions in the model include that the mixing model assumes "perfect" mixing in the airspace, which is inaccurate (despite the high airflow and turnover rate) because of the narrow geometry of the airspace, residence times for air in the box at different locations, and inlet and outlet locations. The Reynolds number for air in the headspace ($Re \sim uL/\upsilon$, where u is the airflow velocity, L is a characteristic dimension of the headspace in the box, and υ is dynamic viscosity of air) is ~10, suggesting nonturbulent flow but not considering that the effects of the inlet conditions (sharp) and the corners of the rectangularly shaped headspace may be turbulence-inducing. However, timescales for free-air diffusive mixing in the headspace ($L^2/D \sim$ 1.5 hr for tracer appearing at the middle of the box) are relatively quick. Nonetheless, the observed breakthrough curves may be substantially affected by the residence time distribution in the headspace.

Transport in the aqueous phase is assumed negligible (i.e., immobile). This is a reasonable assumption since diffusion coefficients for the tracers are orders of magnitude smaller in the aqueous phase, and velocities will also be smaller; in fact, many pores may be at residual saturation with zero relative permeability. The model also neglects condensation of chloroform. Chloroform is generally liquid at room temperature (boiling point 61°C at standard pressure), but we vaporized it before injection by applying a vacuum. Condensation may cause additional effective retardation of chloroform. The use of SF_6 avoids the extra issues with chloroform partitioning and condensation.

Diffusion coefficients are assumed homogeneous and isotropic. This may be a poor assumption for the heated cases, as the reality is a very hot region surrounded by a sharp temperature decline. While the heater is at 260ºC and the sides of the box are 25–32ºC, for the hot case an "average" diffusion coefficient of D_0 at 75ºC is used. Similarly, H_d at 75ºC is used. The model is not tested for sensitivity to these assumptions. The dispersion component of effective diffusivity is also unknown. This affects only the heated case and is expected to impart an anisotropy to the effective diffusivity. The unknown longitudinal dispersivity is wrapped into D^*. This unusual choice of notation (where we fit $\tau_{eff}D_0$ as opposed to $D_{eff} = \tau D_0 + D_L$) is made simply to avoid adding an additional uncertain parameter, D_L. Thus τ_{eff}, the fitting parameter in this model, is not strictly just tortuosity. Depending on Peclet number, this choice of notation could lead to fitted τ_{eff} greater than 1, but we do not find that to be the case. We do see a jump in τ_{eff} for the heated cases compared to the diffusion-only cases and propose that the cause is dispersion.

There are alternative approaches to the model developed here, both analytical and numerical, that would solve some or most of these issues. Analytical alternatives include using superposition theory to handle the air boundary, or convolving Laplace domain transfer functions to handle mixing in the airspace (e.g., *Reimus et al*., 2003). Although the model could be significantly improved with these approaches, due to other geometrical simplifications the resulting parameter estimation will still suffer from significant uncertainties. Numerical alternatives that improve on the simple model performed here include using a simple isothermal finite difference model with appropriate boundaries and allowing for heterogeneous properties, or using an advanced numerical code that correctly handles the equations of state, temperature-dependent diffusivity and Henry's law partitioning, heterogeneous properties, relative permeabilities, and three-phase (salt, water, air) processes. This will be done in future work.

3.3 Post-Test Forensics

Following Experiment 0 (preliminary testing, including several months of moisture movement with and without ventilation and 24 hours of heating to 250ºC), the salt was excavated from the box and sampled for moisture content and thin section. Qualitative observations were made of zones of salt consolidation (Figure 20). Consolidation generally increased with depth, with the exception of the top layer which had an ~1-1.5" thick crust layer that held together well. The heater in this preliminary experiment had been placed near the top of the box (seen in Figure 20), and a completely dry, unconsolidated region with slight brown discoloration formed around the heater.

Samples were collected from a vertical line near the edge of the box. The samples were immediately weighed, then oven-dried and re-weighed. Moisture content by weight is shown in Figure 21. The bottom sample was taken from the ponded, saturated layer. With an assumed grain density for salt of 2165 kg/m^3, the moisture content by weight corresponds to a saturation of $S = 1$ if porosity $\phi = 21\%$ (more consolidated than the initial porosity of ~45%).

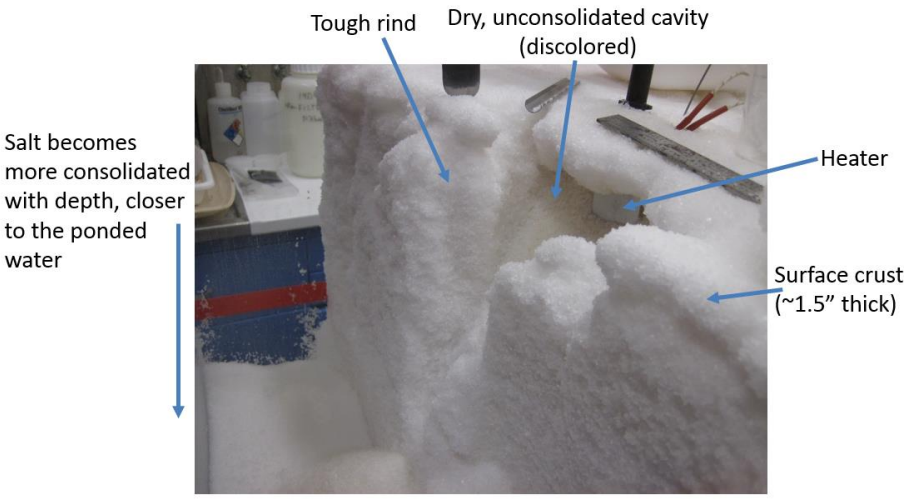

Figure 20. Excavation of Experiment 0; observations of zones of salt consolidation.

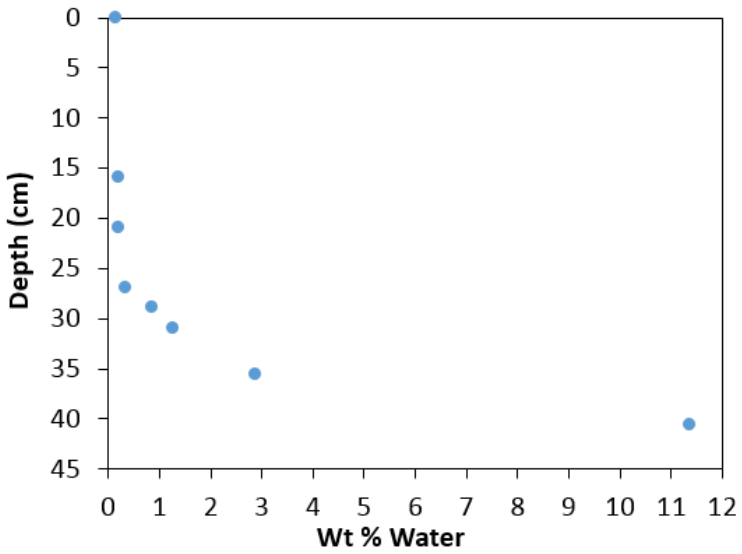

Figure 21. Moisture content with depth in the excavated Experiment 0 salt box.

Experiment 1 has also been forensically examined. The qualitative observations were somewhat different than before. In this case, there was no observed surface crust, perhaps because the ventilated condition had been more consistently maintained for most of the experiment. The heater, which was buried lower than in Experiment 0 and run at 260°C for approximately 2 weeks, was found to have only a slightly more consolidated layer around it, although samples have been sent for thin section to look for evidence of porosity change or precipitation and dissolution of the grains. As before, a region around the heater was discolored and unconsolidated (Figure 22), although it held together significantly better than the dry, loose region seen in Experiment 0 (which was much closer to the top of the salt and ventilated air). The bottom of the box became significantly more consolidated than in Experiment 0, with lithified salt up to a depth of 5-6". This region likely built up significantly during the week between tracer tests T3 and T4, when the breakthrough curve became significantly more delayed

(the injection port is within the tough layer that developed). The saturated layer dropped to 1" above the bottom of the box (when the experiment began, the ponded layer extended 2.5" above the bottom). A tough rind of 0.5-1" thick built up on the sides of the box, beginning a few inches from the top (Figure 23).

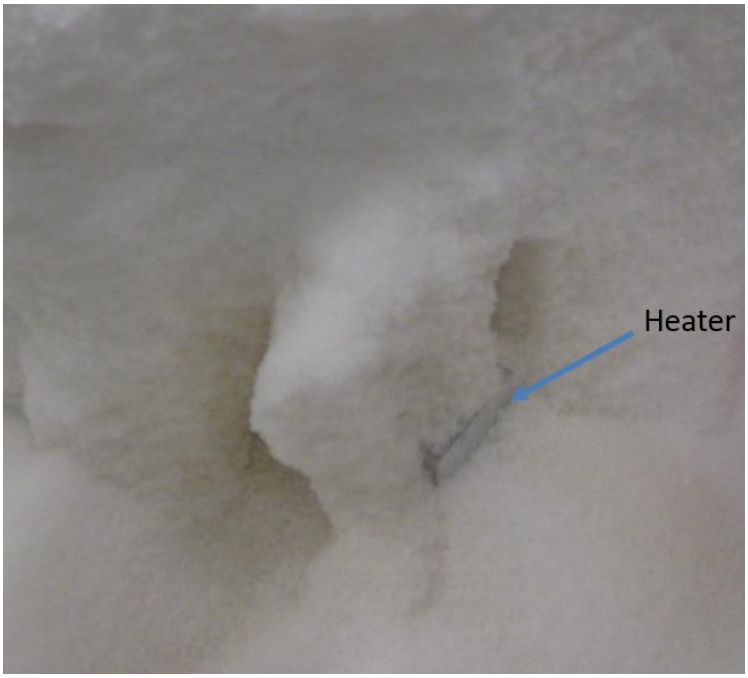

Figure 22. Discolored region around the heater. Some very slight consolidation was observed, as well as some looseness of the salt immediately surrounding the heater. The loose region was significantly firmer and smaller than in Experiment 0 (Figure 20).

Figure 23. Tough rind along the edges of the salt box.

Moisture content with depth was measured for Experiment 1 (Figure 24). In this case, the measured moisture content in the saturated later corresponds to S = 1 if ϕ is around 17%. Porosity based on thin section analysis for the consolidated layer suggests ϕ = 21%.

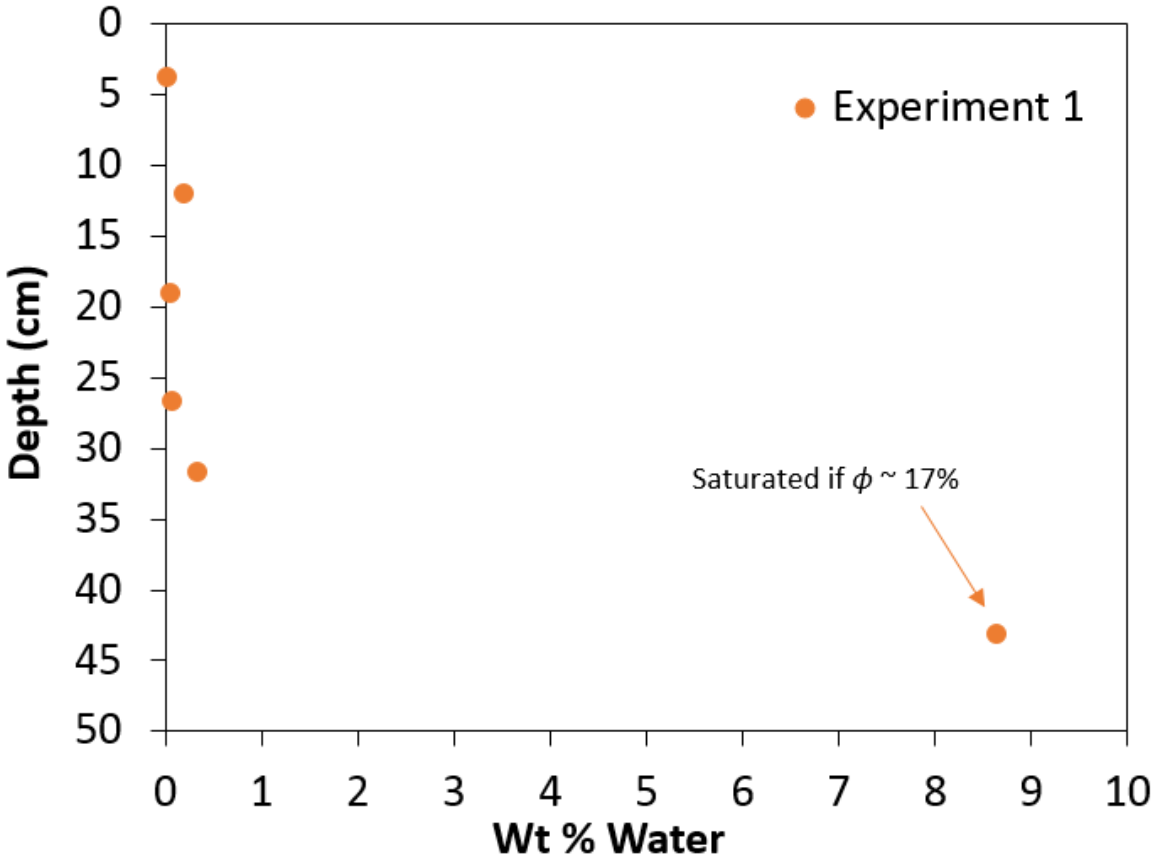

Figure 24. Moisture content with depth in the excavated Experiment 1 salt box.

Thin sections were taken from various locations in the box for Experiment 1. Figure 25 is a transmitted light image of thin section sample SS-22 showing dissolution and re-precipitation of salt grains in sample.

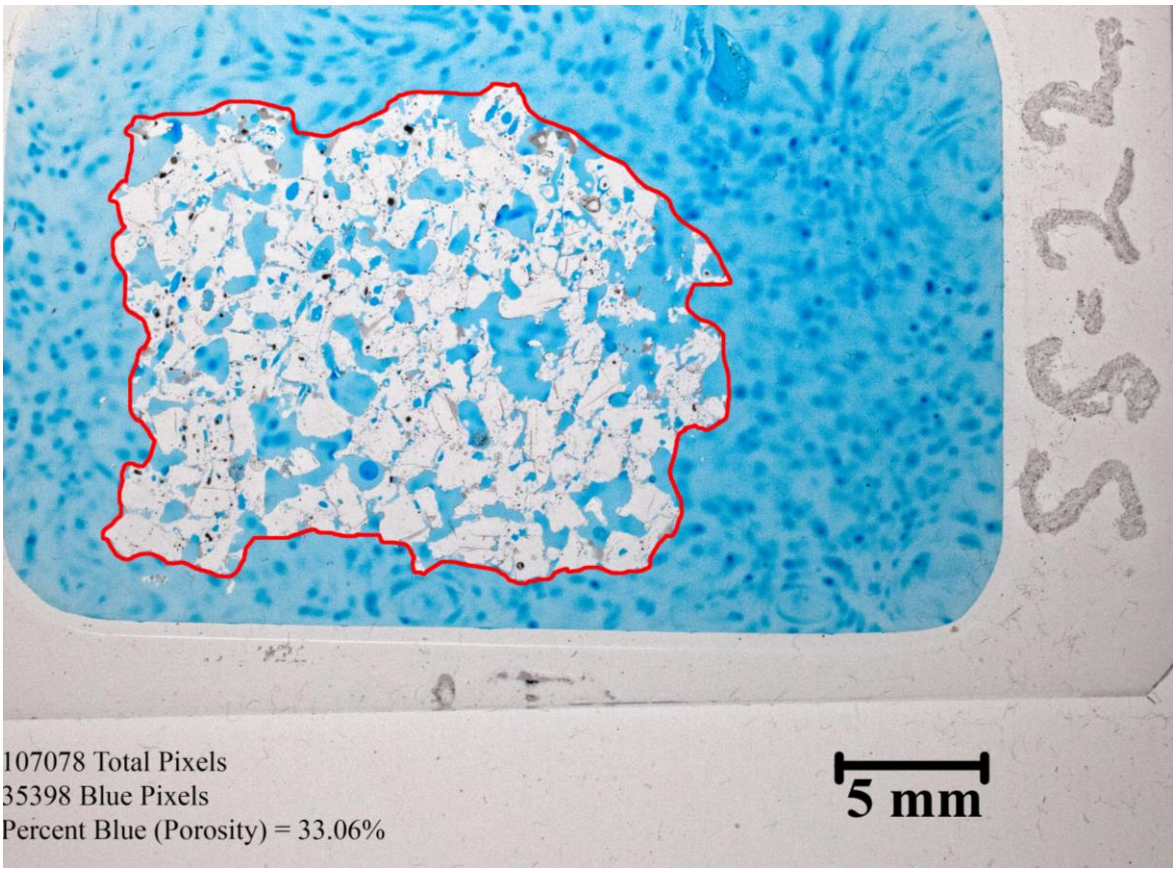

Figure 25. Transmitted light image of Sample SS-22 showing dissolution and re-precipitation of salt grains in sample.

Table 8 describes the porosity values calculated from color injected epoxy thin sections. Although thin section porosity values range from 21.8 to 59.4%, the samples are mostly disaggregated salt crystals. Only samples SS-17, SS-22, and SS-23 represent true porosity values.

Sample #	Porosity (%)	Petrographic description
SS-10	39.63	Slight dissolution on grain corners, no re-precipitation
SS-11	37.71	Slight dissolution on grain corners, no re-precipitation
SS-12	37.35	very little dissolution on grain corners, no re-precipitation
SS-13	47.35	very little dissolution on grain corners, no re-precipitation
SS-14	59.36	Slight dissolution on grain corners, slight re-precipitation
SS-15	57.18	Slight dissolution on grain corners, modest re-precipitation
SS-16	57.88	Slight dissolution on grain corners, no re-precipitation
SS-17	21.76	obvious dissolution and re-precipitation, salt indurated
SS-18	41.14	No dissolution on grain corners, no re-precipitation
SS-19	51.15	Slight dissolution on grain corners, modest re-precipitation
SS-20	50.36	Slight dissolution on grain corners, no re-precipitation
SS-21	59.05	Slight dissolution on grain corners, no re-precipitation
SS-22	33.06	obvious dissolution and re-precipitation, salt indurated
SS-23	45.55	obvious dissolution and re-precipitation, salt indurated
SS-24	43.43	Slight dissolution on grain corners, no re-precipitation

Table 8. Calculated porosity and petrographic description of dissolution/ precipitation behavior.

3.4 Water vapor behavior

The draft test plan included proposed individual-process experiments to study the hygroscopic and diffusive behavior of water in RoM salt, as well as evaporation rates as a function of environmental conditions (including ventilation). Due to time and budget constraints the experiments performed to date have all taken place in the large box, instead of, e.g., column experiments designed to isolate individual processes. However, during Experiment 0 the unheated behavior of water vapor was observed while setting up and testing the equipment for the first heated experiment. In particular, the relative humidity was monitored in the air space above the box while the airflow was repeatedly turned off and on, while monitoring for temperature and relative humidity of the air in. The results are shown in Figure 26 for two cases

separated by over 2 months (69 days). The tests begin when the airflow is stopped after achieving an equilibrium ventilated relative humidity of ~30%.

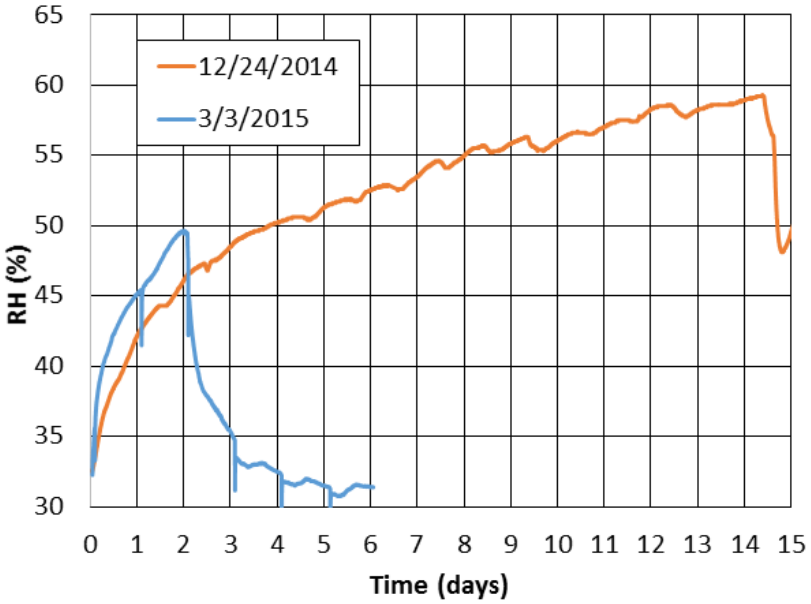

Figure 26. Relative humidity in the airspace during equipment and ventilation testing (Experiment 0). In both cases the airflow is stopped on day 0. Ponded water at the bottom of the salt box provides a moisture supply and the airspace relative humidity climbs in the absence of ventilation.

During the test on 12/24/14, the relative humidity of the airspace increases much more slowly than the later test, on 3/3/15, after a significant period of additional testing and work in the box (but no heating). During this time, ventilation of the box was not controlled or recorded; the box was used for various tests and was sometimes closed without airflow; sometimes closed with airflow; and sometimes open to the laboratory air. That is, it first took 1-2 weeks for the water vapor front to migrate through the box from the ponded water at the bottom, while a later test shows a significantly faster rise (but was not allowed to complete to the expected equilibrium relative humidity). Concurrently, a chloroform tracer test performed with no airflow shows a much faster rise to breakthrough in the airspace (within 1 day; Figure 27). The hygroscopic nature of salt prevents the expected water vapor diffusivity based on its free-air diffusion coefficient and the tortuosity expected in an inert medium. As months pass and the salt/water system becomes more equilibrated throughout the box, the rise towards equilibrium occurs faster. While this very preliminary data set does not allow full exploration of the parameters and timescales involved, it suggests a line of study for a future column experiment. Our numerical models do not currently handle this process but could easily be adapted with a sorption coefficient for water vapor onto the solid.

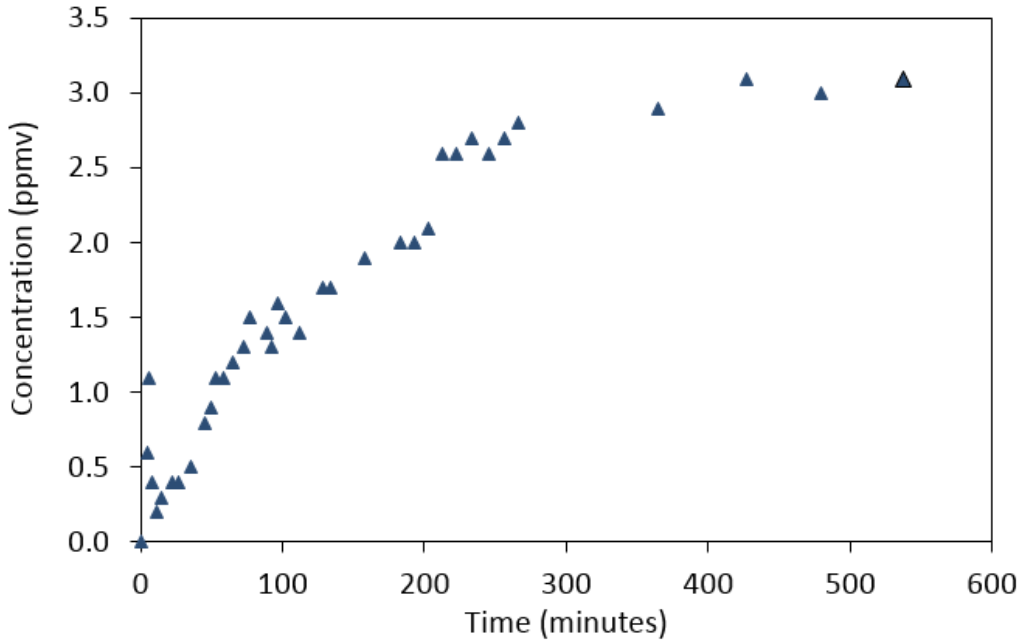

Figure 27. Chloroform breakthrough during Experiment 0 during a test with no airflow.

4. Conclusions

The goals of the laboratory experimental work presented here are to understand processes operating in heated granular salt for which there is still much uncertainty, and to use these data to validate numerical models that will then be used to make useful predictions about moisture, temperature, and structural change at larger scales. The experiments performed to date offer promising insights into water vapor and brine transport in heated salt, including porosity change and hygroscopic retardation of water vapor. The initial data also suggest that gas tracers may be used to probe structural changes in the granular salt during the course of an experiment.

The experimental setup consisted of a bench-scale acrylic box containing granular salt of relatively uniform grain diameter. The box was first filled with salt, instrumented, and tested to see how the system would behave under heating and how to perform post-test forensics. During this testing, relative humidity monitoring in the air under conditions of changing ventilation provided information about water vapor transport through the hygroscopic salt. The first breakthrough curve for relative humidity rebound when airflow was shut off showed a much slower approach to the expected equilibrium relative humidity above brine than a curve taken 2 months later after various states of ventilated and unventilated conditions. The water vapor breakthrough curve was significantly delayed compared to a chloroform breakthrough curve. These results are preliminary and will be the subject of future work (section 5).

The experimental results show the utility of tracer gas tests for experiments with variable internal porosity and structural change. While the analytical model presented here has significant limitations and does not produce accurate parameters, the approach is useful for interpreting results and observing the timing of an otherwise unobservable event (the rate of porosity change in a system that cannot be sampled forensically until after the experiment is completed).

Experiment 1 was the first full, rigorous heated experiment including tracer tests of chloroform and SF_6. The heater was placed 15 cm above the ponded water line and heated to

260ºC for 15 days. Temperature distribution in the box was measured using three bundles of thermocouples with vertical spacing of several inches throughout the salt. Before, during, and after heating, gas tracers were injected into a port at the center of the box just above the water line. The gases were monitored in the airspace with an airflow rate of approximately two turnovers per hour in the volume of air above the salt. Breakthrough curves from Experiment 1 were analyzed using a simple hybrid model combining an analytical solution to the advection-dispersion equation with a discretized air mixing model. The following results were found:

- A convective velocity term in the simplified model (z-direction, vertical velocity only) was required to fit the breakthrough curves during the heated cases, but not during the pre-test Experiment 1 cool case. The model curves for the Experiment 1 post-test cool case were not as good of a fit as the pre-test, possibly due to increased heterogeneity.
- Including temperature-dependent retardation due to Henry's Law partitioning in the model was an effective method for handling chloroform behavior, on the basis of compared model best-fit parameters between chloroform and SF_6. A similar approach may be used for water vapor, once an effective retardation coefficient due to hygroscopic behavior is determined.
- Breakthrough curves for chloroform and SF_6 became significantly more delayed during and after heating, requiring smaller and smaller effective tortuosities to fit the data.
- Salt reconsolidation was observed in post-test forensics in a thick layer between the ponded water line and the heater.

During Experiment 2, the injection port became clogged and tracer tests were stopped after the first heated run with chloroform and SF_6. Therefore, a similar breakthrough curve analysis as in Experiment 1 (e.g., pre- and post-test comparison) could not be performed. However, the results from Experiment 2 were highly illuminating as the data suggest evidence for heat pipe activity, as seen by the flatter temperature gradient, hotter temperatures on the box walls, and extra visible moisture in the box.

The experiments have been a success in terms of making progress towards the overall objectives, but much work remains to be done. Lessons learned during these efforts will be applied to more laboratory tests in the future.

5. Future Work

From the preliminary testing (Experiment 0), we began to observe the effects of water vapor retardation as a function of the hygroscopic behavior of salt (Figure 26). Future work using simpler column-type experiments will continue to explore this phenomenon while avoiding the difficulty of setting up, filling and disposing of hundreds of pounds of salt; it will also simplify model comparisons. Effective retardation coefficients (time-dependent, hysteretic) for water vapor due to hygroscopic behavior in salt could be backed out of best-fit porous media diffusive model parameters for chloroform or SF_6.

The use of isotopic water tracers (e.g., D_2O and $H_2{}^{18}O$) will provide additional information that will fill important gaps between the tracers previously used (chloroform, SF_6) and the primary gas of interest (water vapor). Column and individual-process experiments will also be performed to isolate other processes with uncertain parameterization (e.g., water vapor removal from ventilation; tortuosity of actual RoM salt). Modeling the breakthrough of the condensable versus noncondensible tracers (e.g., SF_6) may also help separate out effects such as enhanced

vapor diffusion (*Ho and Webb,* 2006). This effect may be particularly important in correctly modeling water vapor migration in a salt repository due to high thermal gradients and vapor pressure lowering due to dissolved salt. Isotopic analysis and interpretation in brine systems can be complicated, which may be a greater factor in impure run-of-mine salt experiments than in pure granular NaCl tests (*Horita,* 1989).

After the desired experimental runs with granular salt have been completed, the procedures developed and lessons learned while using the store-bought salt will be applied to a similar experiment using screened RoM salt from WIPP. Individual processes may be tested in a column apparatus while vapor/liquid cycling will be studied in the 2 ft by 2 ft box. Using real RoM salt will provide a more relevant exploration of parameters to feed numerical models, but additional complications arise from using impure salt, including production of acidic vapors under heating, and heterogeneous grain size. The choice of maximum grain diameter when sieving the RoM salt will affect the experiment results and its applicability for use in upscaled models. These issues will be explored.

The second primary objective of the experimental work, which is validating numerical models to be used for prediction of salt behavior during larger-scale experiments and repository operation, has not yet been completed. Preliminary modeling results suggested that temperatures would be hotter at greater distances from the heater, and that porosity change would be roughly spherically symmetric around the heater (*Jordan et al.,* 2014). Since the experiments differed from these early preliminary model results, confirming the nature of the discrepancies between the experiment and numerical model is a substantial effort that will be completed during future work.

REFERENCES

Bechthold, W., E. Smailos, S. Heusermann, W. Bollingerfehr, B. Sabet, T. Rothfuchs, P. Kamlot, J. Grupa, S. Olivella, and F.D. Hansen. 2004. Backfilling and sealing of underground repositories for radioactive waste in salt (Bambus II project). Final Report for European Atomic Energy Community EUR 20621, Office for Official Publications of the European Communities, Luxembourg.

Birkholzer, J.T. 2004. Estimating liquid fluxes in thermally perturbed fractured rock using measured temperature profiles. *J. Hydrol.* 327 (3-4): 496-515, doi 10.1016/j.jhydrol.2005.11.049.

Birkholzer, J.T. and Y.W. Tsang. 2000. Modeling the thermal-hydrologic processes in a large-scale underground heater test in partially saturated fractured tuff. *Water Resour. Res.* 36(6): 1431-1447.

Bodvarsson, G.S., W. Boyle, R. Patterson, and D. Williams. 1999. Overview of scientific investigations at Yucca Mountain—the potential repository for high-level nuclear waste. *J. Contam. Hydrol*. 38 (1): 3–24, doi 10.1016/S0169-7722(99)00009-1.

Brady R., C. Herrick, K. Kuhlman, B. Malama, M. Schuhen, and B. Stenson. 2013. Sandia Experimental Programs Background and Targeted Activities for Forensic Investigation of Rooms B and A1. NE Milestone M4FT-13SN0818036.

Bruckler, L., B.C. Ball, and P. Renault. 1989. Laboratory estimation of gas diffusion coefficient and effective porosity in soils. *Soil Science*, 147(1): 1-10.

Caporuscio, F.A., H. Boukhalfa, M.C. Cheshire, A.B. Jordan, and M. Ding. 2013. Brine Migration Experimental Studies for Salt Repositories, FCRD Used Fuel Disposition Campaign Milestone FCRD-UFD-2013-000204, September 25, 2013.

Cinar, Y., G. Pusch, and V. Reitenbach. 2006. Petrophysical and capillary properties of compacted salt. *Transp. Porous Media* 64 (2): 199-228.

Clayton, D.J., and C.W. Gable. 2009. 3-D Thermal Analyses of High Level Waste Emplaced in a Generic Salt Repository. Sandia National Laboratories Report SAND2009-0633P. Albuquerque, NM.

Domalski, E.S., and E.D. Hearing. Condensed Phase Heat Capacity Data. In: P.J. Linstrom and W.G. Mallard, editors, **NIST Chemistry WebBook, NIST Standard Reference Database Number 69**. National Institute of Standards and Technology, Gaithersburg, MD. http://webbook.nist.gov (accessed 13 July 2015).

Doughty, C., and K. Pruess. 1990. A similarity solution for two-phase fluid and heat flow near high-level nuclear waste packages emplaced in porous media. *Int. J. Heat Mass Transfer* 33(6): 1205–1222.

Eppelbaum, L. V., I. Kutasov, and A. Pilchin. 2014. Applied Geothermics. Springer Science + Business Media LLC, New York, NY.

Freeze, R.A., and J.A. Cherry. 1979. Groundwater. Prentice Hall, Englewood Cliffs, NJ.

Hansen, F.D., and C.D. Leigh. 2012. Salt disposal of heat-generating nuclear waste. Sandia National Laboratories Report SAND2011-0161. Albuquerque, NM.

Hansen, F.D., C.D. Leigh, W. Steininger, W. Bollingerfehr, and T. Von Berlepsche. 2015. Proceedings of the 5th US/German Workshop on Salt Repository Research Design and Operation. Sandia National Laboratories Report SAND2015-0500R. Albuquerque, NM.

Hemond, H.F., and E.J. Fechner. 1999. Chemical Fate and Transport in the Environment. Elsevier Science, Atlanta, GA.

Ho, C.K., and S.W. Webb (Eds.). 2006. Gas transport in porous media (Vol. 20). Springer, Dordrecht, The Netherlands.

Horita, J. 1989. Analytical aspects of stable isotopes in brines. *Chemical Geology: Isotope Geoscience section, 79*(2): 107-112.

Jin, Y., and J.A. Jury. 1996. Characterizing the dependence of gas diffusion coefficient on soil properties. *Soil Science Society of America Journal, 60*(1): 66-71.

Jordan, A.B., P.H. Stauffer, D.T. Reed, H. Boukhalfa, F.A. Caporuscio, and B.A. Robinson. 2014. Draft Test Plan for Brine Migration Experimental Studies in Run-of-Mine Salt Backfill. Los Alamos National Laboratory Report LA-UR-14-27338. Los Alamos, NM.

Jordan, A.B., H. Boukhalfa, F.A. Caporuscio, B.A. Robinson, and P.H. Stauffer. 2015. Hydrous Mineral Dehydration around Heat-Generating Nuclear Waste in Bedded Salt Formations. *Environmental Science & Technology* 49 (11): 6783–6790, **doi** 10.1021/acs.est.5b01002.

Jury, W.A., and R. Horton. 2004. Soil Physics, 6th ed. John Wiley & Sons, Hoboken, NJ.

Kelly, W.R. 1985. Brine migration in salt: Topical report. http://pbadupws.nrc.gov/docs/ML0404/ML040410467.pdf (accessed 10 July 2013).

Krumhansl, J.L., C.L. Stein, G.D. Jarrell, and K.M. Kimball. 1991. Summary of WIPP Room B heater test brine and backfill material data. Sandia National Laboratories Report, SAND-90-0626.

Kuhlman, K.L., and B. Malama. 2013. Brine Flow in Heated Geologic Salt. Sandia National Laboratories Report SAND2013-1944. Albuquerque, NM.

Lappin, A.R. 1988. Summary of site-characterization studies conducted from 1983 through 1987 at the Waste Isolation Pilot Plant (WIPP) site, southeastern New Mexico. In: Post, R.G; High-level waste and general interest: Volume II, p. 371-376. Waste Management: Symposium on Radioactive Waste Management, Tucson, AZ, 28 Feb – 3 Mar 1988.

Marrero, T.R., and E.A. Mason. 1972. Gaseous diffusion coefficients. *Journal of Physical and Chemical Reference Data, 1*(1): 3-118.

Millington, R.J., and J.P. Quirk. 1961. Permeability of porous solids. *Trans. Faraday Soc*. 57: 1200–1207.

Neuzil, C.E. 2013. Can Shale Safely Host US Nuclear Waste? *Trans.,Am. Geophys. Union* 94(30): 261–262.

Olivella, S., S. Castagna, E.E. Alonso, and A. Lloret. 2011. Porosity variations in saline media induced by temperature gradients: experimental evidences and modeling. *Transport in porous media*, 90(3): 763-777.

Pollock, D.W. 1986. Simulation of Fluid Flow and Energy Transport Processes Associated With

High-Level Radioactive Waste Disposal in Unsaturated Alluvium. *Water Resources Research*, 22(5): 765-775.

Reimus, P., G. Pohll, T. Mihevc, J. Chapman, M. Haga, B. Lyles, S. Kosinski, R. Niswonger, and P. Sanders. 2003. Testing and parameterizing a conceptual model for solute transport in a fractured granite using multiple tracers in a forced-gradient test. *Water Resour. Res., 39*(12).

Robinson, B.A., N.Z. Elkins, and J.T. Carter. 2012. Development of a US Nuclear Waste Repository Research Program in Salt. *Nuclear Technology*, 180(1): 122-138.

Rutqvist, J., D. Barr, R. Datta, A. Gens, A. Millard, S. Olivella, C.-F. Tsang, and Y. Tsang. 2005. Coupled thermal–hydrological–mechanical analyses of the Yucca Mountain Drift Scale Test—Comparison of field measurements to predictions of four different numerical models. *International Journal of Rock Mechanics and Mining Sciences*, 42(5): 680-697.

Sander, R. 2015. Henry's law constants. In: P.J. Linstrom and W.G. Mallard, editors, NIST Chemistry WebBook, NIST Standard Reference Database Number 69**.** National Institute of Standards and Technology, Gaithersburg, MD. http://webbook.nist.gov (accessed 22 April 2015).

Silverman, T.S. 1999. A pore-scale experiment to evaluate enhanced vapor diffusion in porous media. Doctoral dissertation, New Mexico Institute of Mining and Technology.

Stauffer, P.H., D.R. Harp, A.B. Jordan, Z. Lu, S. Kelkar, Q. Kang, J. Ten Cate, H. Boukhalfa, Y. Labayed, P.W. Reimus, F.A. Caporuscio, T.A. Miller, and B.A. Robinson. 2013. Coupled model for heat and water transport in a high level waste repository in salt; Los Alamos National Laboratory Document, LA-UR-13-27584. http://www.energy.gov/sites/prod/files/2013/12/f5/CouplModelHeatWaterTransprtGenericHLWRepSalt_1.pdf.

Stauffer, P.H., A.B. Jordan, D.J. Weaver, F.A. Caporuscio, J.A. Ten Cate, H. Boukhalfa, B.A. Robinson, D.C. Sassani, K.L. Kuhlman, E.L. Hardin, S.D. Sevougian, R.J. MacKinnon, Y. Wu, T.A. Daley, B.M. Freifeld, P.J. Cook, J. Rutqvist, and J.T. Birkholzer. 2015. Test proposal document for phased field thermal testing in salt; FCRD Used Fuel Disposition Campaign Milestone FCRD-UFD-2015-000077, April 30, 2015.

Watts, H. 1971. Temperature dependence of the diffusion of carbon tetrachloride, chloroform, and methylene chloride vapors in air by a rate of evaporation method. *Canadian Journal of Chemistry, 49*(1): 67-73.